potentials of liposomes and lipoplexes were determined by a Zetasizer Nano ZS instrument (Malvern Instrument, Ltd., Worcestershire, UK).

2.4. Harvesting of mouse peritoneal macrophages

Mouse peritoneal macrophages were harvested and cultured according to our previous report [16]. Briefly, the macrophages were harvested from mice at 4 days after intraperitoneal injection of 2.9% thioglycolate medium (1 mL). The collected macrophages were washed and suspended in RPMI-1640 medium supplemented with 10% FBS, 100 IU/mL penicillin, 100 μg/mL streptomycin and 2 mM L-glutamine, and plated on culture plates. After incubation for 2 h at 37 °C in 5% CO_2, non-adherent cells were washed off with culture medium, and the macrophages were incubated for another 72 h.

2.5. In-vitro gene transfection

After the macrophages were collected and incubated for 72 h, the culture medium was replaced with Opti-MEM I containing bubble lipoplexes (5 μg pDNA). The macrophages were exposed to US (frequency, 2.062 MHz; duty, 50%; burst rate, 10 Hz; intensity 4.0 W/cm^2) for 20 s using a 6 mm diameter probe placed in the well at 5 min after addition of bubble lipoplexes. In the transfection using naked pDNA and BLs, at 5 min after addition of naked pDNA (5 μg) and BLs (60 μg total lipids) were added, and the macrophages were immediately exposed to US. US was generated using a Sonopore-4000 sonicator (NEPA GENE, Chiba, Japan). Then, 1 h later, the incubation medium was replaced with RPMI-1640 and incubated for an additional 23 h. Lipofectamine® 2000 (Invitrogen, Carlsbad, CA, USA) was used according to the recommended procedures, and the exposure time of Lipofectamine® 2000 was 1 h, which is the same exposure time in other experiments using lipoplexes. Following incubation for 24 h, the cells were scraped from the plates and suspended in lysis buffer (0.05% Triton X-100, 2 mM EDTA, 0.1 M Tris, pH 7.8). Then, the cell suspension was shaken, and centrifuged at 10,000g, 4 °C for 10 min. The supernatant was mixed with luciferase assay buffer (Picagene, Toyo Ink Co., Ltd., Tokyo, Japan) and the luciferase activity was measured in a luminometer (Lumat LB 9507, EG&G Berthold, Bad Wildbad, Germany). The luciferase activity was normalized with respect to the protein content of cells. The protein concentration was determined with a Protein Quantification Kit (Dojindo Molecular Technologies, Inc., Tokyo, Japan). The level of luciferase mRNA expression was determined by RT-PCR.

2.6. Inhibitory experiments of endocytosis in vitro

Endocytosis was inhibited by chlorpromazine (50 μM) as clathrin-mediated endocytosis inhibitor [22], genistein (200 μM) as caveolae-mediated endocytosis inhibitor [23] and 5-(*N*-ethyl-*N*-isopropyl)amiloride (EIPA, 50 μM) as macropinocytosis inhibitor [24]. Each endocytosis inhibitor was added to the macrophages at 30 min before the addition of lipoplexes.

2.7. Fluorescence photographs of pDNA in mouse peritoneal macrophages

To visualize the cellular association of pDNA by fluorescence microscopy (Biozero BZ-8000, KEYENCE, Osaka, Japan), lipoplexes were constructed with TM-rhodamine-labeled pDNA prepared by a Label IT Nucleic Acid Labeling Kit (Mirus Co., Madison, WI, USA).

2.8. Evaluation of cytotoxic effects by MTT assay

The cytotoxicity was evaluated by MTT assay. Briefly, 3-(4,5-dimethyl-2-thiazol)-2,5-diphenyltetrazolium bromide (MTT, Nacalai Tesque, Inc., Kyoto, Japan) solution was added to each well and incubated for 4 h. The resultant formazan crystals were dissolved in 0.04 M HCl-isopropanol and sonicated for 10 min in a bath sonicator. Absorbance values at 550 nm (test wavelength) and 655 nm (reference wavelength) were measured and the results were expressed as viability (%).

2.9. In-vivo gene transfection

Four-week-old ICR female mice were intravenously injected with 400 μL bubble lipoplexes via the tail vein using a 26-gauge syringe needle at a dose of 50 μg pDNA. At 5 min after the injection of bubble lipoplexes, US (frequency, 1.045 MHz; duty, 50%; burst rate, 10 Hz; intensity 1.0 W/cm^2; time, 2 min) was exposed transdermally to the abdominal area using a Sonopore-4000 sonicator with a probe of diameter 20 mm. In the transfection using naked pDNA and BLs, at 4 min after intravenous injection of BLs (500 μg total lipid), naked pDNA (50 μg) was intravenously injected and US was exposed at 1 min after naked pDNA injection. At predetermined times after injection, mice were sacrificed and their organs collected for each experiment. The organs were washed twice with cold saline and homogenized with lysis buffer (0.05% Triton X-100, 2 mM EDTA, 0.1 M Tris, pH 7.8). The lysis buffer was added in a weight ratio of 5 mL/g for the liver or 4 mL/g for the other organs. After three cycles of freezing and thawing, the homogenates were centrifuged at 10,000g, 4 °C for 10 min. The luciferase activity of resultant supernatant was determined by luciferase assay and the level of luciferase mRNA expression was determined by RT-PCR.

2.10. In-vivo imaging

At 6 h after transfection, anesthetized mice were administrated D-luciferin (10 mg/300 μL PBS) (Promega Co., Madison, WI, USA). At 10 min after injection of D-luciferin, organs were excised and luminescent images were taken by NightOWL LB 981 NC instrument (Berthold Technologies, GmbH, Bad Wildbad, Germany). The pseudocolor luminescent images were generated, overlaid with organ images and the luminescence representation was obtained using WinLight software (Berthold Technologies GmbH, Bad Wildbad, Germany).

2.11. Separation of mouse hepatic PCs and NPCs

The separation of mouse hepatic PCs and NPCs was performed according to our previous reports [19]. Briefly, at 6 h after in-vivo transfection using bubble lipoplexes and US exposure, each mouse was anesthetized with pentobarbital sodium (40 ~ 60 mg/kg) and the liver was perfused with perfusion buffer (Ca^{2+}, Mg^{2+}-free HEPES solution, pH 7.2) for 10 min. Then, the liver was perfused with collagenase buffer (HEPES solution, pH 7.5 containing 5 mM $CaCl_2$ and 0.05% (w/v) collagenase (type I)) for 5 min. Immediately after the start of perfusion, the vena cava and aorta were cut and the perfusion rate was maintained at 5 mL/min. At the end of perfusion, the liver was excised. The cells were dispersed in ice-cold Hank's-HEPES buffer by gentle stirring and then filtered through cotton mesh sieves, followed by centrifugation at 50g for 1 min. The pellets containing the hepatic PCs were washed five times with Hank's-HEPES buffer by centrifuging at 50g for 1 min. The supernatant containing the hepatic NPCs was similarly centrifuged 5 times and the resulting supernatant was centrifuged twice at 300g for 10 min. Then, the PCs and NPCs were resuspended separately in ice-cold Hank's-HEPES buffer.

2.12. Isolation of mouse splenic CD11c$^+$ cells

The isolation of mouse splenic CD11c$^+$ cells was performed according to our previous reports [25]. Briefly, At 6 h after in-vivo transfection using bubble lipoplexes and US exposure, the splenic cells were suspended in ice-cold RPMI-1640 medium on ice. Red blood cells were removed by incubation with hemolytic reagent (0.15 M NH_4Cl, 10 mM $KHCO_3$, 0.1 mM EDTA) for 3 min at room temperature. The CD11c$^+$ cells were isolated by magnetic cell sorting with anti-mouse CD11c (N418) microbeads and auto MACS (Miltenyi Biotec, Inc., Auburn, CA, USA) following the manufacturer's instructions.

2.13. Quantitative RT-PCR

Total RNA was isolated from separated cells using a GenElute Mammalian Total RNA Miniprep Kit (Sigma-Aldrich, St. Louis, MO, USA). Reverse transcription of mRNA was carried out using a PrimeScript® RT reagent Kit (Takara Bio Inc., Shiga, Japan). Real-time PCR was performed using SYBR® Premix Ex Taq (Takara Bio Inc., Shiga, Japan) and Lightcycler Quick System 350S (Roche Diagnostics, Indianapolis, IN, USA) with primers. The primers for luciferase and gapdh cDNA were constructed as follows: primer for luciferase cDNA, 5′-TTCTTCGCCAAAAGCACTC-3′ (forward) and 5′-CCCTCGGGTGTAATCAGAAT-3′ (reverse); primer for gapdh, 5′-TCTCCTGCGACTTCAACA-3′ (forward) and 5′-GCTGTAGCCGTATTCATTGT-3′ (reverse) (Sigma-Aldrich, St. Louis, MO, USA). The mRNA copy numbers were calculated for each sample from the standard curve using the instrument software ('Arithmetic Fit Point analysis' for the Lightcycler). The results were expressed as the ratio of luciferase mRNA copy numbers to the housekeeping gene (gapdh) mRNA copy numbers.

2.14. Tissue distribution of radio-labeled pDNA

Lipoplexes constructed with ^{32}P-labeled pDNA ([α-^{32}P]-dCTP, PerkinElmer, Inc., MA, USA) [26] were injected intravenously into mice. At predetermined times after injection, blood was collected from the vena cava under pentobarbital anesthesia. Then, mice were sacrificed and the organs were collected, rinsed with saline and weighed. The tissues were dissolved in Soluene-350 and the resultant lysates were decolorized with isopropanol and 30% H_2O_2, and then neutralized with 5 N HCl. The radioactivity of ^{32}P-labeled pDNA was measured in scintillation counter (LSA-500, Beckman Coulter, Inc., CA, USA) after addition of Clear-Sol I solution.

2.15. Measurement of transaminase activity in the serum

At predetermined times after transfection, the serum was collected from the anesthetized mice. Alanine aminotransferase (ALT) and aspartate aminotransferase (AST) activities in the serum were determined using Transaminase CII-Test Wako kit (Wako Pure Chemical Industries Ltd., Tokyo, Japan) according to manufacturer's instructions.

2.16. Antigen presenting assay

The evaluation of antigen presentation on MHC class I molecules in the splenic dendritic cells was performed by in-vitro antigen presentation assay using CD8-OVA1.3 cells, which are T cell hybridomas with specificity for OVA. The $CD11c^+$ cells isolated from immunized mice were plated in a 96-well plate at various cells numbers and co-cultured with CD8-OVA1.3 cells (1×10^5) for 20 h. The antigen presentation on MHC class I molecules was evaluated by IL-2 secreted from activated CD8-OVA1.3 cells measured by a commercial IL-2 ELISA Kit (Bay bioscience Co., Ltd., Hyogo, Japan).

2.17. Evaluation of OVA-specific cytokine secretion from the splenic cells

At 2 weeks after the last immunization, the splenic cells collected from immunized mice were plated in 96-well plates and incubated for predetermined times at 37 °C in the presence or absence of OVA (100 μg). IFN-γ and IL-4 in the culture medium were measured by the commercial ELISA Kit, respectively (Bay bioscience Co., Ltd., Hyogo, Japan).

2.18. OVA-specific CTL assay

At 2 weeks after the last immunization, the splenic cells harvested from immunized mice were plated in 6-well plates and co-incubated with mitomycin C-treated E.G7-OVA cells or EL4 cells for 4 days. After co-incubation, non-adherent cells were collected, washed and plated in 96-well plates with target cells (E.G7-OVA cells or EL4 cells) at various effector/target (E/T) ratios. The target cells were labeled with ^{51}Cr by incubating with $Na_2^{51}CrO_4$ (PerkinElmer, Inc., MA, USA) in culture medium for 1 h at 37 °C. At 4 h after incubation, the plates were centrifuged and the resultant supernatant of each well was collected and the radioactivity of released ^{51}Cr was measured in a gamma counter. The percentage of ^{51}Cr release was calculated as follows: specific (lysis (%) = [(experimental ^{51}Cr release − spontaneous ^{51}Cr release)/(maximum ^{51}Cr release − spontaneous ^{51}Cr release)] × 100). The percentage of OVA-specific ^{51}Cr release was calculated as (% of ^{51}Cr release from E.G7-OVA cells) − (% of ^{51}Cr release from EL4 cells).

2.19. Therapeutic effects

C57BL/6 mice were immunized three times biweekly. At 2 weeks after last immunization, E.G7-OVA cells and EL4 cells were transplanted subcutaneously into the back of mice. The tumor growth and survival of mice were monitored up to 80 days after transplantation of E.G7-OVA cells and EL4 cells.

2.20. Statistics

Results were presented as the mean ± SD of more than three experiments. Analysis of variance (ANOVA) was used to test the statistical significance of differences among groups. Two-group comparisons were performed by the Student's *t*-test. Multiple comparisons between control groups and other groups were performed by the Dunnett's test and multiple comparisons between all groups were performed by the Tukey-Kramer test.

3. Results

3.1. In-vitro gene transfection properties by Man-PEG_{2000} lipoplexes

Polyethylene-glycol (PEG) modification of particles is necessary to enclose US imaging gas stably and to prepare the

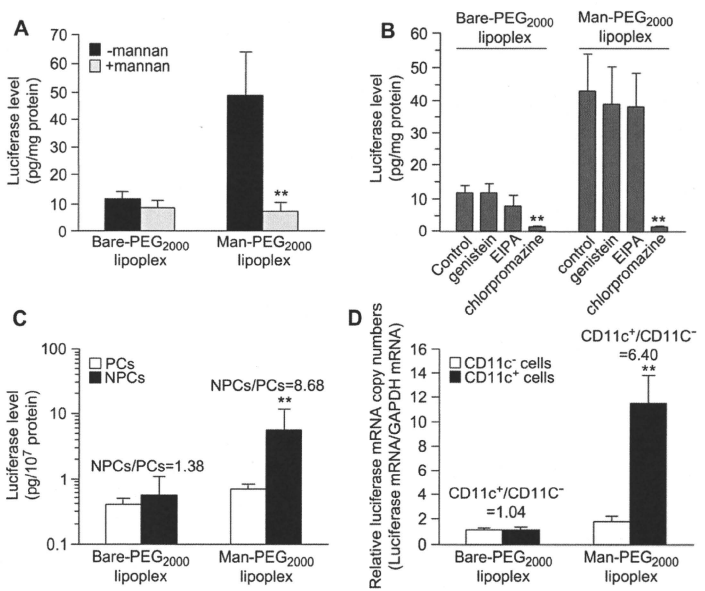

Fig. 2. The mannose receptor-expressing cell-selective gene expression by Man-PEG_{2000} lipoplexes containing Man-PEG_{2000} lipids in vitro and vivo. (A) The level of luciferase expression obtained by Bare-PEG_{2000} lipoplexes and Man-PEG_{2000} lipoplexes (5 μg pDNA) in the absence or presence of 1 mg/mL mannan in mouse cultured macrophages at 24 h after transfection. $^{**}p < 0.01$, compared with the corresponding group of mannan. (B) Inhibition of luciferase expression obtained by Bare-PEG_{2000} lipoplexes and Man-PEG_{2000} lipoplexes (5 μg pDNA) in addition of various endocytosis inhibitors in mouse cultured macrophages at 24 h after transfection. $^{**}p < 0.01$, compared with the corresponding group of control. (C) The level of luciferase expression in mouse hepatic PCs and NPCs after intravenous administration of Bare-PEG_{2000} lipoplexes and Man-PEG_{2000} lipoplexes (50 μg pDNA) in mice at 6 h after transfection. $^{**}p < 0.01$, compared with the corresponding group of PCs. (D) The level of luciferase mRNA expression in mouse splenic $CD11c^+$ cells and $CD11c^-$ cells after intravenous administration of Bare-PEG_{2000} lipoplexes and Man-PEG_{2000} lipoplexes (50 μg pDNA) in mice at 6 h after transfection. $^{**}p < 0.01$, compared with the corresponding group of $CD11c^-$ cells. Each value represents the mean + SD ($n = 3$–4).

small-sized microbubbles for in-vivo administration [12]. Firstly, we developed mannose-conjugated PEG_{2000}-modified lipids (Man-PEG_{2000}-DSPE (Fig. 1)) to prepare the APC-targeted small-sized microbubbles and determined the in-vitro and in-vivo transfection characteristics of mannose-conjugated PEG_{2000}-modified lipoplexes (Man-PEG_{2000} lipoplexes) containing Man-PEG_{2000} lipids. The particle sizes and zeta potentials of Man-PEG_{2000} lipoplexes and non-modified PEG_{2000}-lipoplexes (Bare-PEG_{2000} lipoplexes) were approximately 150 nm and +40 mV, respectively (Supplementary Table 1). In mouse cultured macrophages expressing mannose receptors abundantly, the level of gene expression obtained by Man-PEG_{2000} lipoplexes were significantly higher than those by Bare-PEG_{2000} lipoplexes (Fig. 2A and B). Then, the level of gene expression obtained by Man-PEG_{2000} lipoplexes was suppressed to same extent as that by Bare-PEG_{2000} lipoplexes in the presence of an excess of mannan (Fig. 2A). Moreover, this level of gene expression obtained by Man-PEG_{2000} lipoplexes was also suppressed to same extent as that by Bare-PEG_{2000} lipoplexes in the presence of chlorpromazine (Fig. 2B), which is the inhibitor of clathrin-mediated endocytosis [22]. These results agreed with the results of cellular association of pDNA (Supplementary Fig. 1), and suggest that Man-PEG_{2000} lipoplexes are taken up into the cells via clathrin-mediated endocytosis following the interaction with mannose receptors.

3.2. In-vivo gene transfection properties by Man-PEG_{2000} lipoplexes

Since the degradation of pDNA by nuclease in the blood is one of the critical factors in the in-vivo gene transfection by intravenously administration of lipoplexes, we investigated the stability of Bare-PEG_{2000} lipoplexes and Man-PEG_{2000} lipoplexes against nucleases. Following electrophoresis of naked pDNA and lipoplexes after incubation with DNase I, although naked pDNA underwent the degradation by DNase I, lipoplexes did not undergo the degradation and retained the complex forms (Supplementary Fig. 2). Then, we investigated the gene expression characteristics of Man-PEG_{2000} lipoplexes in the liver and spleen, which are the targeted organs of mannose-modified carriers [27]. In this study, liver was separated in the parenchymal cells (PCs) and non-parenchymal cells (NPCs), and spleen was separated in the dendritic cells ($CD11c^+$ cells) and other cells ($CD11c^-$ cells). As shown in Fig. 2C and D, following intravenous administration of Man-PEG_{2000} lipoplexes, selective gene expression was observed in the hepatic NPCs and the splenic $CD11c^+$ cells, which are the APCs expressing mannose receptors abundantly [28–30].

3.3. In-vitro gene transfection efficiency by Man-PEG_{2000} bubble lipoplexes and US exposure

Although Man-lipoplexes showed the APC-selective gene transfection properties in vivo, this level of gene expression was

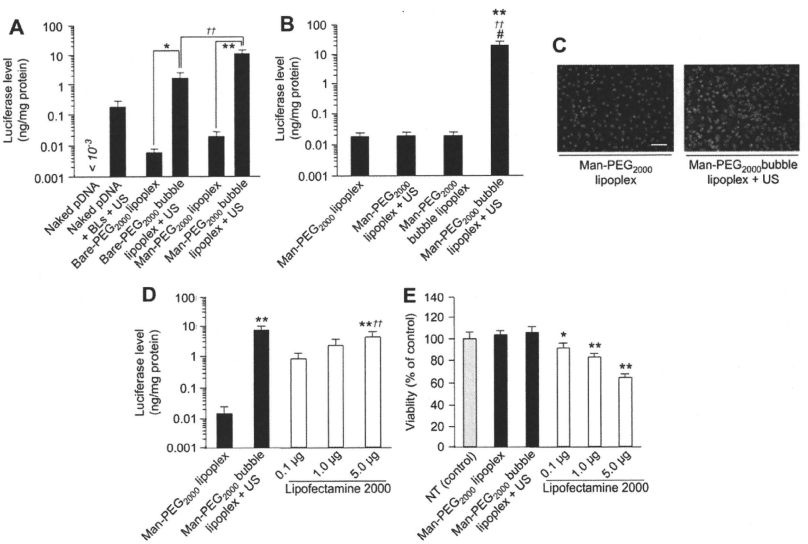

Fig. 3. Enhancement of gene expression by Man-PEG_{2000} bubble lipoplexes and US exposure in vitro. (A) The level of luciferase expression obtained by naked pDNA, naked pDNA + BLs with US exposure, Bare-PEG_{2000} lipoplexes, Bare-PEG_{2000} bubble lipoplexes with US exposure, Man-PEG_{2000} lipoplexes and Man-PEG_{2000} bubble lipoplexes with US exposure (5 μg pDNA) at 24 h after transfection. Significant difference; $^*p < 0.05$; **, $^{\dagger\dagger}p < 0.01$. (B) The level of luciferase expression obtained by Man-PEG_{2000} lipoplexes and Man-PEG_{2000} bubble lipoplexes with or without US exposure (5 μg pDNA) at 24 h after transfection. $^{**}p < 0.01$, compared with Man-PEG_{2000} lipoplex, $^{\dagger\dagger}p < 0.01$, compared with Man-$PEG_{2000}$ lipoplex + US, $^{\#\#}p < 0.01$, compared with Man-PEG_{2000} bubble lipoplex. (C) Representative fluorescent images of cellular association of pDNA obtained by Man-PEG_{2000} lipoplexes and Man-PEG_{2000} bubble lipoplexes with US exposure (5 μg pDNA) at 2 h after treatment. Lipoplexes were constructed with TM-rhodamine-labeled pDNA. TM-rhodamine-labeled pDNA (red), nuclei counterstained by DAPI (blue). Scale bars, 100 μm. (D) Comparison of the level of luciferase expression obtained by Man-PEG_{2000} bubble lipoplexes (5 μg pDNA) and US exposure with that by Lipofectamine 2000. $^{**}p < 0.01$, compared with Man-PEG_{2000} lipoplexes, $^{\dagger\dagger}p < 0.01$, compared with Lipofectamine 2000 (0.1 μg). (E) Comparison of cell viability by transfection using Man-PEG_{2000} bubble lipoplexes (5 μg pDNA) and US exposure with that by Lipofectamine 2000. N.T., non-treatment. $^*p < 0.05$; $^{**}p < 0.01$, compared with N.T. Each value represents the mean + SD ($n = 4$).

low compared with our previous reports [1,19,25]. To enhance the level of gene expression by sonoporation method, we developed Man-PEG$_{2000}$ bubble lipoplexes (Fig. 1) by enclosing US imaging gas (perfluoropropane gas) into Man-PEG$_{2000}$ lipoplexes. The lipid composition of lipoplexes is important for the stable enclosure of US imaging gas. Following optimization of lipid composition, lipoplexes constructed with the saturated lipids only, which have a high melting temperature (T_m), were enclosed US imaging gas stably (Supplementary Table 2). Following enclosure of US imaging gas in lipoplexes, lipoplexes became cloudy and their particle sizes were increased (from 150 nm to 550 nm, approximately) (Supplementary Fig. 3A and Table 3). Then, since the zeta potentials of bubble lipoplexes were lower than that of bubble liposomes and same as that of lipoplexes (Supplementary Tables 1 and 3), it is considered that pDNA is attached on the surface of bubble liposomes. Moreover, the stability against nucleases observed in Man-PEG$_{2000}$ lipoplexes (Supplementary Fig. 2) was maintained after enclosure of US imaging gas into lipoplexes (Supplementary Fig. 3B).

The level of gene expression obtained by Man-PEG$_{2000}$ bubble lipoplexes and US exposure was 500-fold higher than that by Man-PEG$_{2000}$ lipoplexes in mouse cultured macrophages expressing mannose receptors abundantly, and also higher than that by non-modified bubble lipoplexes (Bare-PEG$_{2000}$ bubble lipoplexes, Fig. 1) and US exposure or conventional sonoporation method using naked pDNA and BLs (Fig. 3A). This enhanced gene expression was observed when bubble lipoplexes and US exposure were used for in-vitro gene transfer (Fig. 3B). The cellular association of pDNA obtained by transfection using Man-PEG$_{2000}$ bubble lipoplexes and US exposure was also 10-fold higher than that by Man-PEG$_{2000}$ lipoplexes, and also higher than that by Bare-PEG$_{2000}$ bubble lipoplexes and US exposure or conventional sonoporation method using naked pDNA and BLs (Fig. 3C and Supplementary Fig. 4A). Moreover, this level of gene expression obtained by Man-PEG$_{2000}$ bubble lipoplexes and US exposure was comparable to that by Lipofectamine® 2000, which is widely used as a gene transfection reagent (Fig. 3D). On the other hand, the cytotoxicity by Man-PEG$_{2000}$ bubble lipoplexes and US exposure was lower than that by Lipofectamine® 2000 (Fig. 3E).

3.4. Intracellular uptake properties of pDNA by Man-PEG$_{2000}$ bubble lipoplexes and US exposure

The gene expression obtained by Man-PEG$_{2000}$ bubble lipoplexes and US exposure was significantly suppressed in the presence of an excess of mannan (Fig. 4A). Therefore, the interaction with mannose receptors on the cell membrane is involved in the gene transfection by Man-PEG$_{2000}$ bubble lipoplexes and US exposure, similar to the gene transfection by Man-PEG$_{2000}$ lipoplexes. On the other hand, unlike Man-PEG$_{2000}$ lipoplexes (Fig. 2B), the gene expression obtained by Man-PEG$_{2000}$ bubble lipoplexes and US exposure was not suppressed in the presence of chlorpromazine (Fig. 4B), which is a clathrin-mediated endocytosis inhibitor [22]. These results agreed with the results of cellular association of pDNA (Supplementary Fig. 4B), and indicated that pDNA delivered by Man-PEG$_{2000}$ bubble lipoplexes was directly introduced into the cytoplasm without mediating endocytosis by the gene transfection using Man-PEG$_{2000}$ bubble lipoplexes and US exposure.

3.5. In-vivo gene transfection efficiency by Man-PEG$_{2000}$ bubble lipoplexes and US exposure

As shown in Fig. 5A and B, the level of gene expression obtained by Man-PEG$_{2000}$ bubble lipoplexes and US exposure was

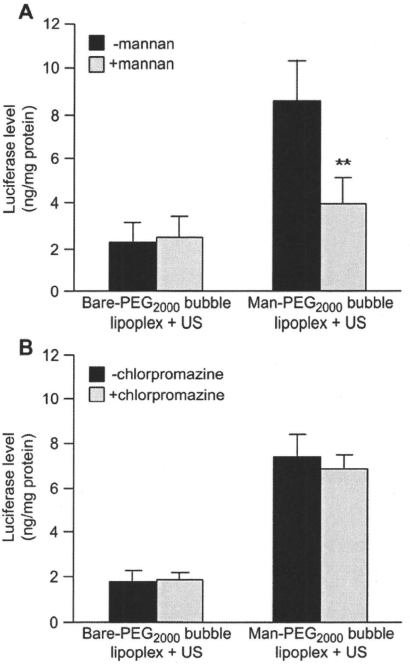

Fig. 4. Effects of mannan and chlorpromazine on gene expression by Man-PEG$_{2000}$ bubble lipoplexes and US exposure in vitro. (A) The level of luciferase expression obtained by Bare-PEG$_{2000}$ bubble lipoplexes with US exposure and Man-PEG$_{2000}$ bubble lipoplexes with US exposure (5 μg pDNA) in the absence or presence of 1 mg/mL mannan at 24 h after transfection. $^{**}p < 0.01$, compared with the corresponding group of mannan. (B) The level of luciferase expression by Bare-PEG$_{2000}$ bubble lipoplexes with US exposure and Man-PEG$_{2000}$ bubble lipoplexes with US exposure (5 μg pDNA) in the absence or presence of 50 μM chlorpromazine at 24 h after transfection. Each value represents the mean + SD ($n = 4$).

500 ~ 800-fold higher than that by Man-PEG$_{2000}$ lipoplexes, and also higher than that by Bare-PEG$_{2000}$ bubble lipoplexes and US exposure or the conventional sonoporation method using naked pDNA and BLs in the liver and spleen, which are the targeted organs of mannose-modified carriers [27]. This enhanced gene expression in the liver and spleen was observed when bubble lipoplexes and US exposure were used for in-vivo gene transfer (Fig. 5C and D). Moreover, this gene expression obtained by Bare-PEG$_{2000}$ bubble lipoplexes with US exposure or Man-PEG$_{2000}$ bubble lipoplexes with US exposure in the liver and spleen remained higher than that by Bare-PEG$_{2000}$ lipoplexes or Man-PEG$_{2000}$ lipoplexes for at least 48 h, respectively (Fig. 5E and F). In addition, the gene expression was also enhanced in the US-exposed organ specifically following gene transfection by direct US exposure to the targeted organ after intravenous administration of Man-PEG$_{2000}$ bubble lipoplexes (Supplementary Fig. 5). On the other hand, the increase of gene expression by bubble lipoplexes and US exposure was not observed in other organ such as lung, kidney and heart (Fig. 5G and H).

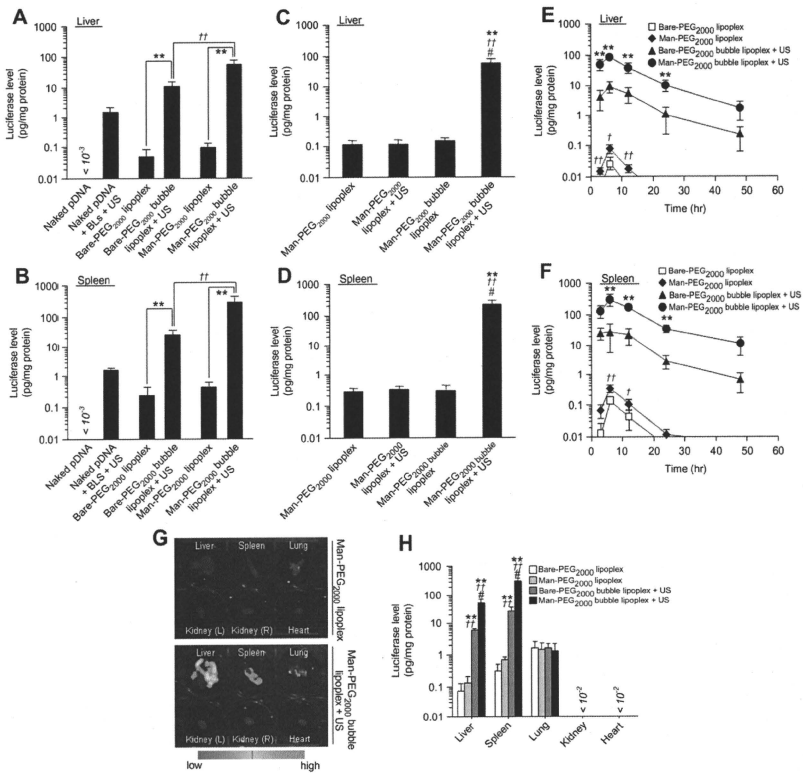

Fig. 5. Enhancement of mannose receptor-expressing cells-selective gene expression by Man-PEG_{2000} bubble lipoplexes and US exposure in vivo. (A, B) The level of luciferase expression obtained by naked pDNA, naked pDNA + BLs with US exposure, Bare-PEG_{2000} lipoplexes, Bare-PEG_{2000} bubble lipoplexes with US exposure, Man-PEG_{2000} lipoplexes and Man-PEG_{2000} bubble lipoplexes with US exposure (50 μg pDNA) in the liver (A) and spleen (B) at 6 h after transfection. Significant difference; **, $^{\dagger\dagger}p < 0.01$. (C, D) The level of luciferase expression obtained by Man-PEG_{2000} lipoplexes and Man-PEG_{2000} bubble lipoplexes with or without US exposure (50 μg pDNA) in the liver (C) and spleen (D) at 6 h after transfection. **$p < 0.01$, compared with Man-PEG_{2000} lipoplex, $^{\dagger\dagger}p < 0.01$, compared with Man-$PEG_{2000}$ lipoplex + US, $^{\#\#}p < 0.01$, compared with Man-PEG_{2000} bubble lipoplex. (E, F) Time-course of luciferase expression in the liver (E) and spleen (F) after transfection by Bare-PEG_{2000} lipoplexes, Man-PEG_{2000} lipoplexes, Bare-PEG_{2000} bubble lipoplexes with US exposure and Man-PEG_{2000} bubble lipoplexes with US exposure (50 μg pDNA). Each value represents the mean ± SD ($n = 4$). **$p < 0.01$, compared with Bare-PEG_{2000} bubble lipoplex + US, $^{\dagger}p < 0.05$; $^{\dagger\dagger}p < 0.01$, compared with Bare-$PEG_{2000}$ lipoplex. (G) In-vivo imaging photographs of luciferase expression in the isolated organs at 6 h after transfection by Man-PEG_{2000} lipoplexes and Man-PEG_{2000} bubble lipoplexes with US exposure (50 μg pDNA). (H) The level of luciferase expression in each organ at 6 h after transfection by Bare-PEG_{2000} lipoplexes, Man-PEG_{2000} lipoplexes, Bare-PEG_{2000} bubble lipoplexes with US exposure and Man-PEG_{2000} bubble lipoplexes with US exposure (50 μg pDNA). **$p < 0.01$, compared with the corresponding group of Bare-PEG_{2000} lipoplex, $^{\#\#}p < 0.01$, compared with the corresponding group of Man-PEG_{2000} lipoplex, $^{\#\#}p < 0.01$, compared with the corresponding group of Bare-PEG_{2000} bubble lipoplex + US. Each value represents the mean + SD ($n = 4$).

3.6. *Targeted cell-selective gene transfection properties by Man-PEG_{2000} bubble lipoplexes and US exposure in vivo*

We investigated the mannose receptor-expressing cell selectivity of gene expression by transfection using Man-PEG_{2000} bubble lipoplexes and US exposure. In the liver, the level of gene expression in the hepatic NPCs expressing mannose receptors was significantly higher than that in the hepatic PCs following gene transfection by Man-PEG_{2000} bubble lipoplexes and US exposure (Fig. 6A). This difference in gene expression between the NPCs and PCs obtained by Man-PEG_{2000} bubble lipoplexes and US exposure was similar to that by Man-PEG_{2000} lipoplexes, although the level of gene expression in the NPCs and PCs was markedly higher. On the other hand, selective gene expression in the NPCs was not observed by Bare-PEG_{2000} bubble lipoplexes and US exposure.

In the spleen, the level of mRNA expression in the $CD11c^+$ cells, which are the splenic dendritic cells expressing mannose receptors, was significantly higher than that in the $CD11c^-$ cells following transfection by Man-PEG_{2000} bubble lipoplexes and US exposure (Fig. 6B). On the other hand, selective gene expression in the $CD11c^+$ cells was not observed by Bare-PEG_{2000} bubble lipoplexes and US exposure.

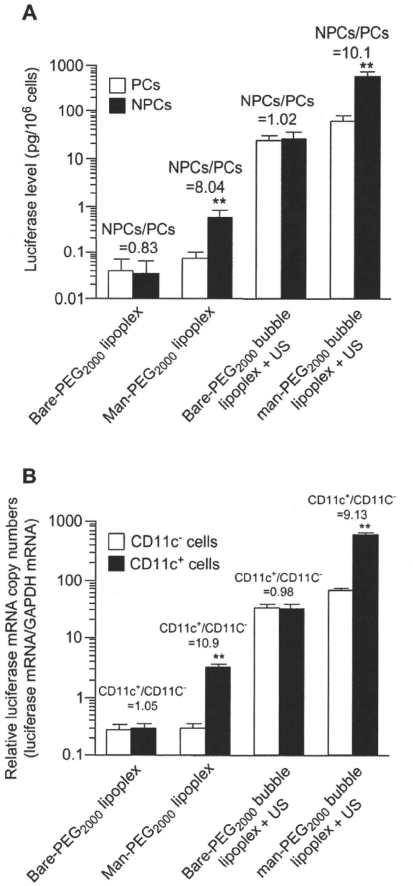

Fig. 6. Hepatic and splenic cellular localization of luciferase expression by Man-PEG_{2000} bubble lipoplexes and US exposure. (A) Hepatic cellular localization of luciferase expression at 6 h after transfection by Bare-PEG_{2000} lipoplexes, Man-PEG_{2000} lipoplexes, Bare-PEG_{2000} bubble lipoplexes with US exposure and Man-PEG_{2000} bubble lipoplexes with US exposure (50 μg pDNA). $^{**}p < 0.01$, compared with the corresponding group of PCs. (B) Splenic cellular localization of luciferase mRNA expression at 6 h after transfection by Bare-PEG_{2000} lipoplexes, Man-PEG_{2000} lipoplexes, Bare-PEG_{2000} bubble lipoplexes with US exposure and Man-PEG_{2000} bubble lipoplexes with US exposure (50 μg pDNA). $^{**}p < 0.01$, compared with the corresponding group of $CD11c^-$ cells. Each value represents the mean + SD ($n = 4$).

3.7. In-vivo distribution properties of pDNA by Man-PEG_{2000} bubble lipoplexes and US exposure

Next, to elucidate the mechanism of enhanced in-vivo gene expression using Man-PEG_{2000} bubble lipoplexes and US exposure, we investigated the effect on the tissue distribution of pDNA followed by gene transfection. In this study, Bare-PEG_{2000} bubble lipoplexes and Man-PEG_{2000} bubble lipoplexes constructed with radio-labeled pDNA were intravenously administrated, and then mice were subjected to external US exposure. As shown in Fig. 7, in the case of both bubble lipoplexes, the retention time of pDNA in the blood was slightly reduced and the distribution of pDNA delivered by bubble lipoplexes was significantly increased by US exposure in the liver and spleen (Fig. 7). Moreover, the amount of pDNA distributed in the liver and spleen by Man-PEG_{2000} bubble lipoplexes and US exposure (Fig. 7A) was higher than that by Bare-PEG_{2000} bubble lipoplexes and US exposure (Fig. 7B). On the other hand, no increase of pDNA distribution followed by US exposure was observed in the lung.

3.8. The liver toxicity by Man-PEG_{2000} bubble lipoplexes and US exposure

We examined ALT and AST activities in the serum to investigate the liver toxicity by gene transfection using Man-PEG_{2000} bubble lipoplexes and US exposure. ALT and AST activities in the serum were increased by gene transfection using Bare-PEG_{2000} lipoplexes and Man-PEG_{2000} lipoplexes. On the other hands, the increase of ALT and AST activities was not observed by gene transfection using Bare-PEG_{2000} bubble lipoplexes and Man-PEG_{2000} bubble lipoplexes with US exposure (Fig. 8).

3.9. Antigen presentation on MHC class I molecules in immunized splenic dendritic cells

To investigate the DNA vaccine effects by Man-PEG_{2000} bubble lipoplexes and US exposure, we prepared Man-PEG_{2000} bubble lipoplexes constructed with pDNA expressing OVA as a model antigen. Firstly, to investigate the antigen (OVA) presentation on MHC class I molecules in the splenic dendritic cells ($CD11c^+$ cells) by Man-PEG_{2000} bubble lipoplexes constructed with pCMV-OVA and US exposure, the splenic $CD11c^+$ cells isolated from once-immunized mice were co-incubated with CD8-OVA1.3 cells, which are T cell hybridomas with specificity for OVA. Following measurement of IL-2 to evaluate the activation of T cells, the IL-2 secretion from activated CD8-OVA1.3 cells co-incubated with the $CD11c^+$ cells isolated from mice immunized by Man-PEG_{2000} bubble lipoplexes and US exposure was the highest of all (Fig. 9A). This result indicates that DNA vaccination by Man-PEG_{2000} bubble lipoplexes constructed with pCMV-OVA and US exposure can induce significantly high $CD8^+$-T lymphocyte activation.

3.10. Antigen-specific cytokine secretion from immunized splenic cells

We evaluated the OVA-specific cytokine secretion from the splenic cells immunized by Man-PEG_{2000} bubble lipoplexes constructed with pCMV-OVA and US exposure. Following optimization of immunization schedule, it was shown that a 2 week interval was necessary to achieve the same level of gene expression as former transfection in the spleen (Supplementary Fig. 6) and at least three times immunization was necessary to effective anti-tumor effects by DNA vaccination using this method (Supplementary Fig. 7). Therefore, the immunization to mice was performed according to the protocol shown in Fig. 9B. As shown in Fig. 9C, in the presence of OVA, the highest amount of IFN-γ (Th1 cytokine) was secreted from splenic cells harvested from mice immunized with Man-PEG_{2000} bubble lipoplexes and US exposure. On the other hand, no secretion of IFN-γ was observed in any of the groups in the absence of OVA. Moreover, the secretion of IL-4 (Th2 cytokine) was not increased in any of the groups both in the presence or absence of OVA (Fig. 9C). These results suggest that immunization by Man-PEG_{2000} bubble lipoplexes constructed with

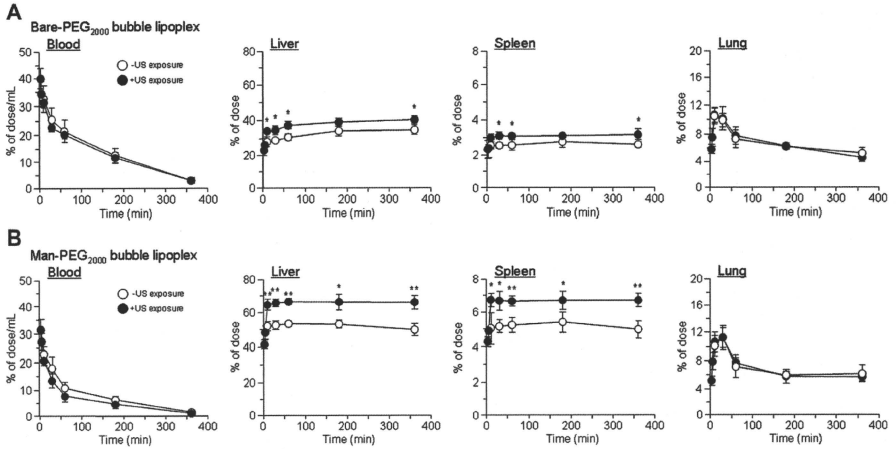

Fig. 7. Tissue distribution of pDNA by Man-PEG_{2000} bubble lipoplexes and US exposure. Tissue distribution after intravenous administration of (A) Bare-PEG_{2000} bubble lipoplexes and (B) Man-PEG_{2000} bubble lipoplexes (50 μg pDNA) with or without US exposure in mice. US was exposed at 5 min after intravenous administration of bubble lipoplexes. Each value represents the mean ± SD ($n = 3$). *$p < 0.05$; **$p < 0.01$, compared with the corresponding group of US exposure.

pCMV-OVA and US exposure significantly enhances the differentiation of helper T cells to Th1 cells, which are pivotal cells for the activation of cytotoxic T lymphocytes (CTL) with high anti-tumor activity, by OVA stimulation.

3.11. Antigen-expressing cell-specific CTL activity in immunized splenic cells

Next, we assessed the CTL activity in the splenic cells harvested from mice immunized by Man-PEG_{2000} bubble lipoplexes and US exposure. Following experiments according to the protocol shown in Fig. 9B, the splenic cells immunized by Man-PEG_{2000} bubble lipoplexes constructed with pCMV-OVA and US exposure showed the highest CTL activity in all groups against E.G7-OVA cells which are the lymphoma cells expressing OVA (Fig. 9D). In contrast, the CTL activity was not observed in EL4 cells which are the lymphoma cells not expressing OVA in all groups (Fig. 9D). These results indicate that the splenic cells immunized by Man-PEG_{2000} bubble lipoplexes constructed with pCMV-OVA and US exposure induce the OVA-expressing cell-specific CTL activity.

3.12. Therapeutic effects against antigen-expressing tumor by DNA vaccination

Finally, we investigated the anti-tumor effects by DNA vaccination using Man-PEG_{2000} bubble lipoplexes and US exposure. Following experiments according to the protocol shown in Fig. 10A, significantly high anti-tumor effects against E.G7-OVA cells were observed in mice immunized by Man-PEG_{2000} bubble lipoplexes constructed with pCMV-OVA and US exposure (Fig. 10B). However, in mice transplanted EL4 cells, no anti-tumor effects were observed in any of the groups (Fig. 10C). Moreover, we investigated the maintenance of DNA vaccine effects following administration of Man-PEG_{2000} bubble lipoplexes and US exposure. According to the protocol shown in Fig. 11A, E.G7-OVA cells were re-transplanted into mice which first-transplanted tumors were completely rejected by DNA vaccination using Man-PEG_{2000} bubble lipoplexes and US exposure. As results, high anti-tumor effects were observed in mice following re-transplantation of E.G7-OVA cells (Fig. 11B); therefore it was demonstrated that DNA vaccine effects obtained by Man-PEG_{2000} bubble lipoplexes constructed with pCMV-OVA and US exposure were maintained for at least 80 days.

4. Discussion

To obtain high therapeutic effects by DNA vaccination using tumor-specific antigen-coding gene, it is essential to transfer the gene selectively and efficiently into the APCs, such as macrophages and dendritic cells [31,32]. However, it is difficult to transfer the gene into the APCs selectively because of the number of APCs is limited in the organ [33]. Since the APCs are expressed a large number of mannose receptors [28,29], we and other groups have developed mannose-modified non-viral carriers for gene delivery to the APCs [7,25,34]. On the other hand, our group also reported that the gene transfection efficiency in the APCs was lower than that in other cells [35]; therefore it is difficult to achieve high gene transfection efficiency to induce high therapeutic effects by DNA vaccination in vivo. In the present study, to establish an APC-selective and efficient gene delivery system, we developed US-responsive and mannose-modified carriers, named Man-PEG_{2000} bubble lipoplexes, which had selectivity to the APCs and responded to US exposure. The gene delivery system using Man-PEG_{2000} bubble lipoplexes and US exposure enabled to achieve markedly high gene expression in macrophages and dendritic cells selectively in vivo, in spite of the handy system used intravenous administration and external US exposure. Moreover, we succeeded in obtaining high anti-tumor effects by applying this method to DNA vaccine therapy using OVA-expressing pDNA.

Firstly, since PEG_{2000}-modification is necessary to enclose US imaging gas stably [12], we prepared Man-PEG_{2000} lipoplexes

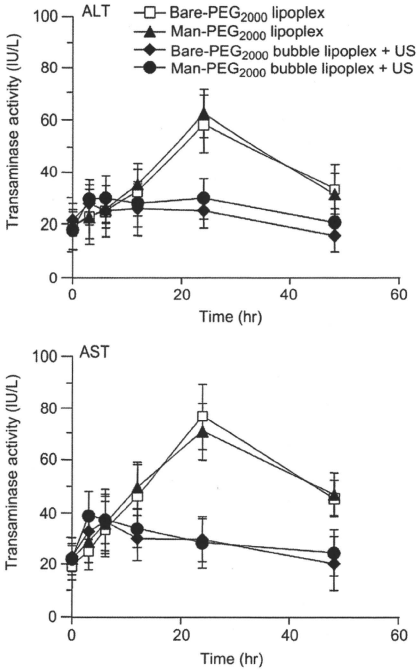

Fig. 8. Liver toxicity by gene transfection using Man-PEG_{2000} bubble lipoplexes and US exposure. Time-course of serum transaminase activities after transfection by Bare-PEG_{2000} lipoplexes, Man-PEG_{2000} lipoplexes, Bare-PEG_{2000} bubble lipoplexes with US exposure and Man-PEG_{2000} bubble lipoplexes with US exposure (50 μg pDNA). Alanine aminotransferase (ALT) and aspartate aminotransferase (AST) in the serum were measured at predetermined times after transfection. Each value represents the mean ± SD ($n = 4$).

containing Man-PEG_{2000} lipids. This Man-PEG_{2000} lipoplexes exhibited mannose receptor-expressing cell-selective gene expression both in vitro and vivo (Fig. 2). On the other hand, the level of gene expression by Man-PEG_{2000} lipoplexes was lower than that by mannosylated lipoplexes without PEG-modification, as reported previously by our group [1,25]. However, this result was considered to be contributed by the reduced interaction with the cell membrane and the reduction of endosomal escape efficiency by PEG_{2000}-modification [36,37]. In the sonoporation method, Tachibana et al. demonstrated that a transient pore is created on the cell membrane followed by the degradation of microbubbles [38]. Then, nucleic acids, such as pDNA, siRNA and oligonucleotides, are introduced into the cell through the generated pore [13,15,16]. Consequently, since the nucleic acids are directly introduced into cytoplasm in the sonoporation method [13,14], it is considered that the low level of transfection efficiency obtained by Man-PEG_{2000} lipoplexes can be overcome by applying sonoporation method. As shown in Figs. 3 and 4, a large amount of pDNA is directly introduced into the cytoplasm and high level of gene expression is observed by gene transfection using Man-PEG_{2000} bubble lipoplexes and US exposure. Therefore, by delivering pDNA to the APCs using Man-PEG_{2000} bubble lipoplexes, it is suggested that high level of gene expression in the APCs can easily achieve by following US exposure in this gene transfection method.

In this study, the level of gene expression obtained by transfection using Man-PEG_{2000} bubble lipoplexes and US exposure was higher than that obtained by Man-PEG_{2000} lipoplexes or Bare-PEG_{2000} bubble lipoplexes with US exposure in the liver and spleen (Fig. 5). Moreover, gene expression by Man-PEG_{2000} bubble lipoplexes and US exposure was observed selectively in the hepatic NPCs and the splenic dendritic cells (Fig. 6), known as mannose receptor-expressing cells [28–30]. Although this selectivity of gene expression was the same as that obtained by mannosylated lipoplexes reported previously by our group [1,25], this level of gene expression was markedly higher. It is considered that this enhanced and cell-selective gene expression is contributed by the increase of interaction with mannose receptor-expressing cells by mannose modification (Supplementary Fig. 1), by the improvement of delivering efficiency of nucleic acids to the targeted organs (Fig. 7) and by the direct introduction of nucleic acids into the cytoplasm of targeted cells followed by US exposure to Man-PEG_{2000} bubble lipoplexes (Figs. 3C and 4B and Supplementary Fig. 4). Moreover, the enhanced gene expression was not observed in the lung, kidney and spleen (Fig. 5G and H). It is guessed that the reason why the enhanced gene expression was not observed in the lung is because US is not spread to the thoracic cavity by the diaphragm, and the reason why the enhanced gene expression was not observed in the kidney and heart was because the distributed amounts of bubble lipoplexes were markedly small. In addition, since the particle size of bubble lipoplexes (approximately 500 nm) is suitable for delivery to the liver and spleen, compared with stabilized liposomes (approximately 100 nm) [39], the gene transfection system using Man-PEG_{2000} bubble lipoplexes and US exposure is a suitable method for the selective delivery of nucleic acids into the mannose receptor-expressing cells in the liver and spleen.

On the other hand, the liver toxicity followed by gene transfection using Man-PEG_{2000} bubble lipoplexes and US exposure was lower than that by Man-PEG_{2000} lipoplexes (Fig. 8). It was reported that the CpG motifs in the pDNA sequence are recognized to Toll-like receptor 9 (TLR9) in the endosomes [40,41]; therefore it has been considered that the production of proinflammatory cytokines, such as TNF-α, IFN-γ and IL-12, could be induced in the lipofection method using liposomes and emulsions, and these cytokines cause liver injury [42]. However, in the gene transfection using Man-PEG_{2000} bubble lipoplexes and US exposure, a large amount of pDNA was directly introduced into the cytoplasm not-mediated endocytosis (Figs. 3C and 4B and Supplementary Fig. 4). Therefore, it is considered that pDNA is not recognized to TLR9 in the endosomes, and consequently liver toxicity followed by transfection using Man-PEG_{2000} bubble lipoplexes and US exposure is low.

In the previous study [16], we developed combination-use method using mannosylated lipoplexes [1] and BLs [12] with US exposure to achieve targeted cell-selective gene transfer. However, this combination-use method is complicated because of the necessity of twice injection of mannosylated lipoplexes and BLs, therefore it is difficult to apply for medical treatments using multiple injection. Moreover, it is considered that the difference of in-vivo distribution characteristics between mannosylated lipoplexes and BLs might be decreased its transfection efficacy. On the other hand, this transfection method using Man-PEG_{2000} bubble lipoplexes and US exposure is handy because of using only once injection of Man-PEG_{2000} bubble lipoplexes and external US exposure. In addition, this method using Man-PEG_{2000} bubble lipoplexes and US exposure overcame the difference of in-vivo distribution of formulations, which might lead to the decrease of

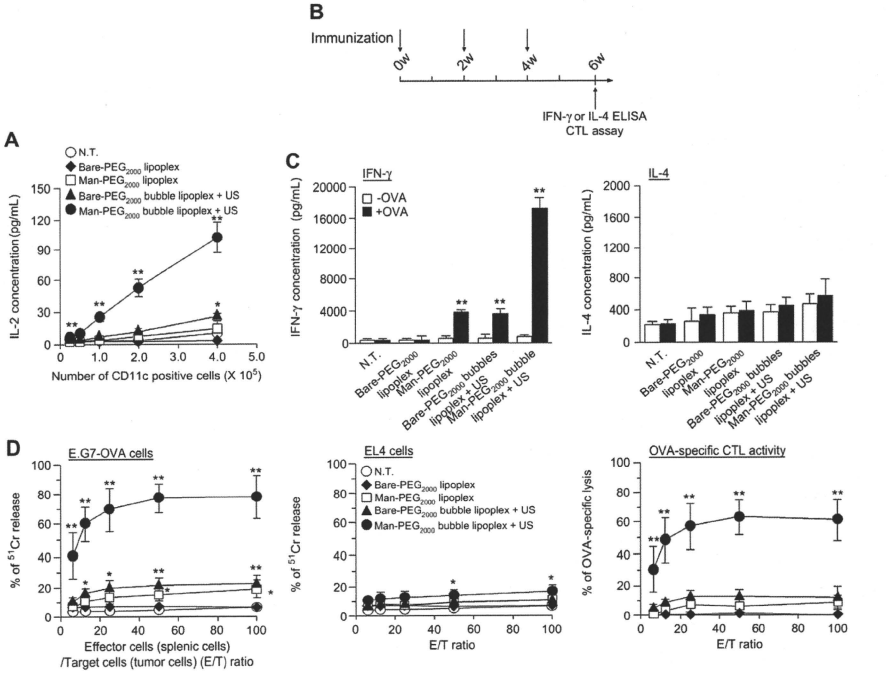

Fig. 9. Cytokine secretion characteristics and CTL activities by DNA vaccination using Man-PEG_{2000} bubble lipoplexes and US exposure. (A) OVA presentation on MHC class I molecules in the splenic $CD11c^+$ cells at 24 h after transfection by Bare-PEG_{2000} lipoplexes, Man-PEG_{2000} lipoplexes, Bare-PEG_{2000} bubble lipoplexes with US exposure and Man-PEG_{2000} bubble lipoplexes with US exposure (50 μg pDNA). OVA presentation on MHC class I molecules was determined by IL-2 level secreted from CD8-OVA1.3 cells co-incubated with the $CD11c^+$ cells isolated from once-immunized mice. Each value represents the mean ± SD ($n = 4$). $^*p < 0.05$; $^{**}p < 0.01$, compared with the corresponding group of N.T. (B) Schedule of immunization for OVA-specific cytokine secretion experiments and CTL assay. (C) OVA-specific IFN-γ and IL-4 secretion from the splenic cells immunized three times biweekly by Bare-PEG_{2000} lipoplexes, Man-PEG_{2000} lipoplexes, Bare-PEG_{2000} bubble lipoplexes with US exposure and Man-PEG_{2000} bubble lipoplexes with US exposure (50 μg pDNA). The splenic cells were collected at 2 weeks after last immunization. After the immunized splenic cells were cultured for 72 h in the absence or presence of 100 μg OVA, IFN-γ and IL-4 secreted in the medium were measured by ELISA. Each value represents the mean + SD ($n = 4$). $^{**}p < 0.01$, compared with the corresponding group of OVA. (D) OVA-specific CTL activities after immunization three times by Bare-PEG_{2000} lipoplexes, Man-PEG_{2000} lipoplexes, Bare-PEG_{2000} bubble lipoplexes with US exposure and Man-PEG_{2000} bubble lipoplexes with US exposure (50 μg pDNA). CTL activities to E.G7-OVA and EL4 cells in the immunized splenic cells were determined by ^{51}Cr release assay. Each value represents the mean ± SD ($n = 4$). $^*p < 0.05$; $^{**}p < 0.01$, compared with the corresponding group of N.T. N.T., non-treatment.

transfection efficiency. In fact, the level of gene expression by this method was higher than that by combination-use method reported previously in the targeted organs (liver and spleen) (Fig. 5) and targeted cells (hepatic NPC and splenic dendritic cells) (Fig. 6); therefore this gene transfection method using Man-PEG_{2000} bubble lipoplexes and US exposure is more suitable for APC-selective gene transfer in vivo.

Since APC-selective and efficient gene expression was observed by transfection using Man-PEG_{2000} bubble lipoplexes and US exposure, effective therapeutic effects are to be expected by applying this transfection method to DNA vaccine therapy, which the targeted cells are the APCs, using tumor-specific antigen-coding pDNA [31,32]. However, since the level of gene expression by transfection using Man-PEG_{2000} bubble lipoplexes and US exposure was reduced sequentially (Supplementary Fig. 6), multiple transfections are essential to obtain more effective vaccine effects against cancer (Supplementary Fig. 7). On the other hand, a 2 week interval was needed to achieve the same level of gene expression by lipoplexes or bubble lipoplexes with US exposure as former transfection in the spleen (Supplementary Fig. 7B and C). Meyer et al. reported that the optimal transfection interval was necessary to achieve high gene expression by the second transfection using lipofection methods because of IFN-γ secretion by intravenous administration of lipoplexes [43]; therefore it is considered that a similar phenomenon is contributed to the sonoporation methods using microbubbles constructed with phospholipids. Based on these findings, we performed the optimization of immunization times (Supplementary Fig. 7) and determined the optimal immunization schedule as shown in Figs. 9B, 10A and 11A.

In DNA vaccine therapy, unlike cancer immunotherapy using tumor-specific antigenic peptides, the peptides expressed as gene products in the cells act as the internal antigen. Since the internal antigens are presented on MHC class I molecules, the strong activation of CTL and high anti-tumor effects are expected in DNA vaccination therapy [44,45]. In this study, by applying this gene transfection method to DNA vaccine therapy using OVA-expressing

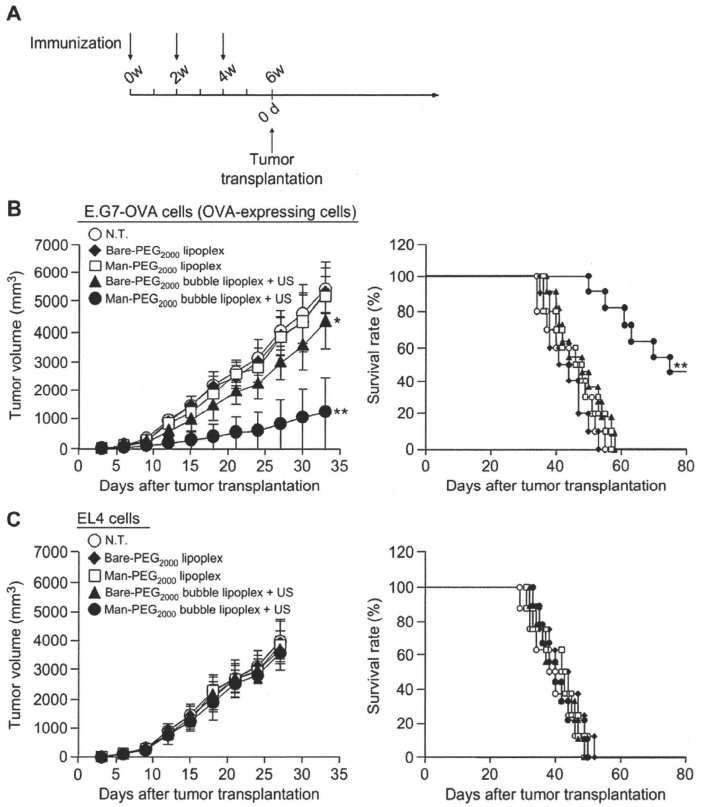

Fig. 10. Anti-tumor effects by DNA vaccination using Man-PEG_{2000} bubble lipoplexes and US exposure. (A) Schedule of immunization for experiments of therapeutic effects. (B, C) Anti-tumor effects by immunization using Bare-PEG_{2000} lipoplexes, Man-PEG_{2000} lipoplexes, Bare-PEG_{2000} bubble lipoplexes with US exposure and Man-PEG_{2000} bubble lipoplexes with US exposure (50 μg pDNA). Two weeks after last immunization, (B) E.G7-OVA cells or (C) EL4 cells (1×10^6 cells) were transplanted subcutaneously into the back of mice ($n = 8$–11). The tumor volume was evaluated (each value represents the mean ± SD) and the survival was monitored up to 80 days after the tumor transplantation. $^*p < 0.05$; $^{**}p < 0.01$, compared with the corresponding group of N.T. N.T., non-treatment.

pDNA, i) the presentation of OVA-peptides on MHC class I molecules of splenic dendritic cells, ii) OVA-specific Th1 cytokine secretion from splenic cells by OVA stimulation and iii) marked activation of CTL against OVA-expressing tumor were observed by gene transfection using Man-PEG_{2000} bubble lipoplexes constructed with pCMV-OVA and US exposure (Fig. 9). Moreover, high and long-term anti-tumor effects against OVA-expressing tumor were observed in mice transfected by Man-PEG_{2000} bubble lipoplexes constructed with pCMV-OVA and US exposure (Figs. 10 and 11). It is considered that these results are contributed by APS-selective and efficient gene transfection efficiency using Man-PEG_{2000} bubble lipoplexes and US exposure. Although more detailed examination by pDNA encoding other tumor-specific antigens, such as gp100 in melanoma or PSA in prostate cancer [45], is necessary, this transfection method by Man-PEG_{2000} bubble lipoplexes and US exposure might be available for DNA vaccine therapy.

The gene transfection method using Man-PEG_{2000} bubble lipoplexes and US exposure was enabled selective and efficient gene transfer to the mannose receptor-expressing cells in the liver such as Kupffer cells and hepatic endothelial cells, which are components of the APCs (Fig. 6A). Therefore, this method is also suitable for anti-inflammatory therapy targeted to Kupffer cells and hepatic endothelial cells, known to play a key role in inflammation [46,47]. In spite of low liver toxicity, since this gene transfection system showed NPC-selective and efficient gene expression in the liver (Fig. 8), better therapeutic effects could be expected by Man-PEG_{2000} bubble lipoplexes constructed with

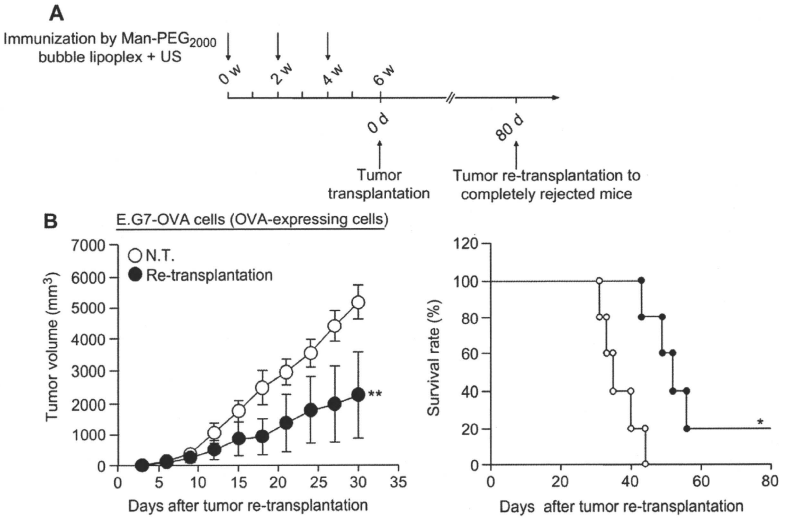

Fig. 11. Maintaining of Anti-tumor effects by DNA vaccination using Man-PEG_{2000} bubble lipoplexes and US exposure. At 80 days after first transplantation of E.G7-OVA cells to immunized mice three times by Man-PEG_{2000} bubble lipoplexes and US exposure, E.G7-OVA cells (1×10^6 cells) were re-transplanted subcutaneously into the back of mice which the first-transplanted tumors were completely rejected ($n = 5$). The tumor volume was evaluated (each value represents the mean ± SD) and the survival was monitored up to 80 days after the tumor re-transplantation. $^*p < 0.05$; $^{**}p < 0.01$, compared with the corresponding group of N.T. N.T., non-treatment.

various types of nucleic acids, such as NF-κB decoy [48], ICAM-1 antisense oligonucleotides [49], with low doses of nucleic acids. Moreover, organ-specific gene expression was observed in US-exposed organ by exposing US to the organ directly after intravenous administration of Man-PEG_{2000} bubble lipoplexes (Supplementary Fig. 5); therefore the beforehand knockdown of inflammatory factors such as NF-κB or ICAM-1 by Man-PEG_{2000} bubble lipoplexes and US exposure might be available for the prevention of ischemia reperfusion injury, a major problem in living donor liver transplantation.

5. Conclusion

In this study, we developed the gene transfection method using Man-PEG_{2000} bubble lipoplexes and US exposure. This transfection method enabled APC-selective and efficient gene expression, and moreover, effective anti-tumor effects was obtained by applying this method to DNA vaccine therapy against cancer. This method could be widely used in a variety of targeted cell-selective and efficient gene transfection methods by substituting mannose with various ligands reported previously [2–6]. In addition, in this gene transfection method, pDNA can directly introduce the nucleic acids into the cells through the transient pores created by US-responsive degradation of bubble lipoplexes, therefore this method could apply to many ligands which are not taken up via endocytosis. These findings make a valuable contribution to overcome the poor introducing efficiency into cytoplasm which is a major obstacle for gene delivery by non-viral vectors, and show that this method is an effective method for in-vivo gene delivery.

Acknowledgements

This work was supported in part by Grant-in-Aid for Scientific Research from the Ministry of Education, Culture, Sports, Science and Technology of Japan, and by Health and Labour Sciences Research Grants for Research on Noninvasive and Minimally Invasive Medical Devices from the Ministry of Health, Labour and Welfare of Japan, and by the Programs for Promotion of Fundamental Studies in Health Sciences of the National Institute of Biomedical Innovation (NIBIO), and by the Japan Society for the Promotion of Sciences (JSPS) through a JSPS Research Fellowship for Young Scientists.

Appendix. Supplementary data

Supplementary data associated with this article can be found, in the online version, at doi:10.1016/j.biomaterials.2010.06.058.

References

[1] Kawakami S, Sato A, Nishikawa M, Yamashita F, Hashida M. Mannose receptor-mediated gene transfer into macrophages using novel mannosylated cationic liposomes. Gene Ther 2000;7:292–9.
[2] Schiffelers RM, Koning GA, ten Hagen TL, Fens MH, Schraa AJ, Janssen AP, et al. Anti-tumor efficacy of tumor vasculature-targeted liposomal doxorubicin. J Control Release 2003;91:115–22.
[3] Torchilin VP, Levchenko TS, Rammohan R, Volodina N, Papahadjopoulos-Sternberg B, D'Souza GG. Cell transfection in vitro and in vivo with nontoxic TAT peptide–liposome–DNA complexes. Proc Natl Acad Sci U S A 2003;100:1972–7.
[4] Kirpotin DB, Drummond DC, Shao Y, Shalaby MR, Hong K, Nielsen UB, et al. Antibody targeting of long-circulating lipidic nanoparticles does not increase tumor localization but does increase internalization in animal models. Cancer Res 2006;66:6732–40.

[5] Goldstein D, Gofrit O, Nyska A, Benita S. Anti-HER2 cationic immunoemulsion as a potential targeted drug delivery system for the treatment of prostate cancer. Cancer Res 2007;67:269–75.
[6] Oba M, Aoyagi K, Miyata K, Matsumoto Y, Itaka K, Nishiyama N, et al. Polyplex micelles with cyclic RGD peptide ligands and disulfide cross-links directing to the enhanced transfection via controlled intracellular trafficking. Mol Pharmacol 2008;5:1080–92.
[7] Sheng KC, Kalkanidis M, Pouniotis DS, Esparon S, Tang CK, Apostolopoulos V, et al. Delivery of antigen using a novel mannosylated dendrimer potentiates immunogenicity in vitro and in vivo. Eur J Immunol 2008;38:424–36.
[8] Satkauskas S, Bureau MF, Puc M, Mahfoudi A, Scherman D, Miklavcic D, et al. Mechanisms of in vivo DNA electrotransfer: respective contributions of cell electropermeabilization and DNA electrophoresis. Mol Ther 2002;5:133–40.
[9] Mukai H, Kawakami S, Kamiya Y, Ma F, Takahashi H, Satake K, et al. Pressure-mediated transfection of murine spleen and liver. Hum Gene Ther 2009;20:1157–67.
[10] Nishikawa M, Nakayama A, Takahashi Y, Fukuhara Y, Takakura Y. Reactivation of silenced transgene expression in mouse liver by rapid, large-volume injection of isotonic solution. Hum Gene Ther 2008;19:1009–20.
[11] Hernot S, Klibanov AL. Microbubbles in ultrasound-triggered drug and gene delivery. Adv Drug Deliv Rev 2008;60:1153–66.
[12] Suzuki R, Takizawa T, Negishi Y, Utoguchi N, Sawamura K, Tanaka K, et al. Tumor specific ultrasound enhanced gene transfer in vivo with novel liposomal bubbles. J Control Release 2008;125:137–44.
[13] Negishi Y, Endo Y, Fukuyama T, Suzuki R, Takizawa T, Omata D, et al. Delivery of siRNA into the cytoplasm by liposomal bubbles and ultrasound. J Control Release 2008;132:124–30.
[14] Lentacker I, Geers B, Demeester J, De Smedt SC, Sanders NN. Design and evaluation of doxorubicin-containing microbubbles for ultrasound-triggered doxorubicin delivery: cytotoxicity and mechanisms involved. Mol Ther 2010;18:101–8.
[15] Liu Y, Miyoshi H, Nakamura M. Encapsulated ultrasound microbubbles: therapeutic application in drug/gene delivery. J Control Release 2006;114:89–99.
[16] Un K, Kawakami S, Suzuki R, Maruyama K, Yamashita F, Hashida M. Enhanced transfection efficiency into macrophages and dendritic cells by the combination method using mannosylated lipoplexes and bubble liposomes with ultrasound exposure. Hum Gene Ther 2010;21:65–74.
[17] Kawabata K, Takakura Y, Hashida M. The fate of plasmid DNA after intravenous injection in mice: involvement of scavenger receptors in its hepatic uptake. Pharm Res 1995;12:825–30.
[18] Potter NS, Harding CV. Neutrophils process exogenous bacteria via an alternate class I MHC processing pathway for presentation of peptides to T lymphocytes. J Immunol 2001;167:2538–46.
[19] Hattori Y, Suzuki S, Kawakami S, Yamashita F, Hashida M. The role of dioleoylphosphatidylethanolamine (DOPE) in targeted gene delivery with mannosylated cationic liposomes via intravenous route. J Control Release 2005;108:484–95.
[20] Hattori Y, Kawakami S, Lu Y, Nakamura K, Yamashita F, Hashida M. Enhanced DNA vaccine potency by mannosylated lipoplex after intraperitoneal administration. J Gene Med 2006;8:824–34.
[21] Lee YC. 2-Imino-2-methoxyethyl 1-thioglycosides: new reagents for attaching sugars to proteins. Biochemistry 1976;15:3956–63.
[22] Wang LH, Rothberg KG, Anderson RG. Mis-assembly of clathrin lattices on endosomes reveals a regulatory switch for coated pit formation. J Cell Biol 1993;123:1107–17.
[23] Akiyama T, Ishida J, Nakagawa S, Ogawara H, Watanabe S, Itoh N, et al. Genistein, a specific inhibitor of tyrosine-specific protein kinases. J Biol Chem 1987;262:5592–5.
[24] West MA, Bretscher MS, Watts C. Distinct endocytotic pathways in epidermal growth factor-stimulated human carcinoma A431 cells. J Cell Biol 1989;109:2731–9.
[25] Hattori Y, Kawakami S, Nakamura K, Yamashita F, Hashida M. Efficient gene transfer into macrophages and dendritic cells by in vivo gene delivery with mannosylated lipoplex via the intraperitoneal route. J Pharmacol Exp Ther 2006;318:828–34.
[26] Rigby PWJ, Dieckmann M, Rhodes C, Berg P. Labeling deoxyribonucleic acid to high specific activity in vitro by nick translation with DNA polymerase I. J Mol Biol 1977;113:237–51.
[27] Kawakami S, Wong J, Sato A, Hattori Y, Yamashita F, Hashida M. Biodistribution characteristics of mannosylated, fucosylated, and galactosylated liposomes in mice. Biochim Biophys Acta 2000;1524:258–65.
[28] Taylor PR, Gordon S, Martinez-Pomares L. The mannose receptor: linking homeostasis and immunity through sugar recognition. Trends Immunol 2005;26:104–10.
[29] Tacken PJ, de Vries IJ, Torensma R, Figdor CG. Dendritic-cell immunotherapy: from ex vivo loading to in vivo targeting. Nat Rev Immunol 2007;7:790–802.
[30] Kurts C. CD11c: not merely a murine DC marker, but also a useful vaccination target. Eur J Immunol 2008;38:2072–5.
[31] Steinman RM, Banchereau J. Taking dendritic cells into medicine. Nature 2007;449:419–26.
[32] Hume DA. Macrophages as APC and the dendritic cell myth. J Immunol 2008;181:5829–35.
[33] Liu K, Waskow C, Liu X, Yao K, Hoh J, Nussenzweig M. Origin of dendritic cells in peripheral lymphoid organs of mice. Nat Immunol 2007;8:578–83.
[34] Abe Y, Kuroda Y, Kuboki N, Matsushita M, Yokoyama N, Kojima N. Contribution of complement component C3 and complement receptor type 3 to carbohydrate-dependent uptake of oligomannose-coated liposomes by peritoneal macrophages. J Biochem 2008;144:563–70.
[35] Sakurai F, Inoue R, Nishino Y, Okuda A, Matsumoto O, Taga T, et al. Effect of DNA/liposome mixing ratio on the physicochemical characteristics, cellular uptake and intracellular trafficking of plasmid DNA/cationic liposome complexes and subsequent gene expression. J Control Release 2000;66:255–69.
[36] Song LY, Ahkong QF, Rong Q, Wang Z, Ansell S, Hope MJ, et al. Characterization of the inhibitory effect of PEG-lipid conjugates on the intracellular delivery of plasmid and antisense DNA mediated by cationic lipid liposomes. Biochim Biophys Acta 2002;1558:1–13.
[37] Deshpande MC, Davies MC, Garnett MC, Williams PM, Armitage D, Bailey L, et al. The effect of poly(ethylene glycol) molecular architecture on cellular interaction and uptake of DNA complexes. J Control Release 2004;97:143–56.
[38] Tachibana K, Uchida T, Ogawa K, Yamashita N, Tamura K. Induction of cell-membrane porosity by ultrasound. Lancet 1999;353:1409.
[39] Ishida O, Maruyama K, Sasaki K, Iwatsuru M. Size-dependent extravasation and interstitial localization of polyethyleneglycol liposomes in solid tumor-bearing mice. Int J Pharm 1999;190:49–56.
[40] Latz E, Schoenemeyer A, Visintin A, Fitzgerald KA, Monks BG, Knetter CF, et al. TLR9 signals after translocating from the ER to CpG DNA in the lysosome. Nat Immunol 2004;5:190–8.
[41] Leifer CA, Brooks JC, Hoelzer K, Lopez J, Kennedy MN, Mazzoni A, et al. Cytoplasmic targeting motifs control localization of toll-like receptor 9. J Biol Chem 2006;281:35585–92.
[42] Tousignant JD, Gates AL, Ingram LA, Johnson CL, Nietupski JB, Cheng SH, et al. Comprehensive analysis of the acute toxicities induced by systemic administration of cationic lipid: plasmid DNA complexes in mice. Hum Gene Ther 2000;11:2493–513.
[43] Meyer O, Schughart K, Pavirani A, Kolbe HV. Multiple systemic expression of human interferon-beta in mice can be achieved upon repeated administration of optimized pcTG90-lipoplex. Gene Ther 2000;7:1606–11.
[44] Donnelly JJ, Wahren B, Liu MA. DNA vaccines: progress and challenges. J Immunol 2005;175:633–9.
[45] Rice J, Ottensmeier CH, Stevenson FK. DNA vaccines: precision tools for activating effective immunity against cancer. Nat Rev Cancer 2008;8:108–20.
[46] Cook-Mills JM, Deem TL. Active participation of endothelial cells in inflammation. J Leukoc Biol 2005;77:487–95.
[47] Kolios G, Valatas V, Kouroumalis E. Role of Kupffer cells in the pathogenesis of liver disease. World J Gastroenterol 2006;12:7413–20.
[48] Higuchi Y, Kawakami S, Yamashita F, Hashida M. The potential role of fucosylated cationic liposome/NFkappaB decoy complexes in the treatment of cytokine-related liver disease. Biomaterials 2007;28:532–9.
[49] Wong J, Kubes P, Zhang Y, Li Y, Urbanski SJ, Bennett CF, et al. Role of ICAM-1 in chronic hepatic allograft rejection in the rat. Am J Physiol Gastrointest Liver Physiol 2002;283:196–203.

Published OnlineFirst July 14, 2010; DOI:10.1158/0008-5472.CAN-10-0184

AACR

Cancer Research

Circadian Rhythm of Transferrin Receptor 1 Gene Expression Controlled by c-Myc in Colon Cancer –Bearing Mice

Fumiyasu Okazaki, Naoya Matsunaga, Hiroyuki Okazaki, et al.

Cancer Res 2010;70:6238-6246. Published OnlineFirst July 14, 2010.

Published OnlineFirst July 14, 2010; DOI:10.1158/0008-5472.CAN-10-0184

Molecular and Cellular Pathobiology

Cancer Research

Circadian Rhythm of Transferrin Receptor 1 Gene Expression Controlled by c-Myc in Colon Cancer–Bearing Mice

Fumiyasu Okazaki[1], Naoya Matsunaga[1], Hiroyuki Okazaki[1], Naoki Utoguchi[2], Ryo Suzuki[2], Kazuo Maruyama[2], Satoru Koyanagi[1], and Shigehiro Ohdo[1]

Abstract

The abundance of cell surface levels of transferrin receptor 1 (TfR1), which regulates the uptake of iron-bound transferring, correlates with the rate of cell proliferation. Because TfR1 expression is higher in cancer cells than in normal cells, it offers a target for cancer therapy. In this study, we found that the expression of TfR1 in mouse colon cancer cells was affected by the circadian organization of the molecular clock. The core circadian oscillator is composed of an autoregulatory transcription-translation feedback loop, in which CLOCK and BMAL1 are positive regulators and the *Period* (*Per*), *Cryptochrome* (*Cry*), and *Dec* genes act as negative regulators. TfR1 in colon cancer–bearing mice exhibited a 24-hour rhythm in mRNA and protein levels. Luciferase reporter analysis and chromatin immunoprecipitation experiments suggested that the clock-controlled gene *c-MYC* rhythmically activated the transcription of the *TfR1* gene. Platinum incorporation into tumor DNA and the antitumor efficacy of transferrin-conjugated liposome-delivered oxaliplatin could be enhanced by drug administration at times when TfR1 expression increased. Our findings suggest that the 24-hour rhythm of TfR1 expression may form an important aspect of strategies for TfR1-targeted cancer therapy. *Cancer Res; 70(15); 6238–46. ©2010 AACR.*

Introduction

In mammals, the master pacemaker controlling the circadian rhythm is located in the suprachiasmatic nuclei of the hypothalamus (1). Regulation of circadian physiology relies on the interplay of interconnected transcription-translation feedback loops. The BMAL1/CLOCK complex activates clock-controlled genes, including *Per, Cry*, and *Dec*, the products of which act as repressors by interacting with BMAL1/CLOCK (2–5). This mechanism also regulates the 24-hour rhythm in output physiology through the periodic activation/repression of clock-controlled output genes in healthy peripheral tissue and tumor tissue (6, 7).

Transferrin receptor 1 (TfR1) is involved in the uptake of iron into cells through the binding and internalization of transferrin, and its regulation by intracellular iron levels has assisted in the elucidation of many important aspects of cellular iron homeostasis (8, 9). Iron is important for metabolism, respiration, and DNA synthesis. Thus, TfR1 is expressed not only in normal healthy cells but also in malignant tumor cells (8, 10). Recently, another TfR-like molecule named TfR2 has been recognized and investigated (11, 12), but the exact function of TfR2 remains unclear (8). It has been reported that the expression of TfR1 in mammary epithelial cells exhibits a significant 24-hour rhythm (13). Such rhythmic variation in TfR1 expression seems to affect its iron uptake function resulting in time-dependent changes in the internalization of iron-loaded Tf. However, it is not clear if the expression of TfR1 in colon cancer cells shows a significant 24-hour rhythm.

Many of the pharmacologic properties of conventional drugs can be improved through the use of an optimized drug delivery system (DDS), which includes particular carriers composed primarily of lipids and/or polymers (14). The high expression of TfR1 in tumor can potentially be used to deliver cytotoxic agents into malignant cells, including chemotherapeutic drugs, cytotoxic proteins (8), and Tf-coupled polyethylene glycol (Tf-PEG) liposomes were designed as intracellular targeting carriers for drugs by systemic administration. In fact, Tf-PEG liposomes encapsulating a platinum (Pt)-based anticancer drug, oxaliplatin, can increase its accumulation in tumor masses (15, 16). On the other hand, daily rhythmic variations in biological functions are thought to affect the efficacy and/or toxicity of drugs: a large number of drugs cannot be expected to have the same potency at different administration times (7, 17). However, it is unclear what influence the rhythmic expression of TfR1 has on the pharmacokinetics/pharmacodynamics of transferrin targeting liposomes.

Authors' Affiliations: [1]Department of Pharmaceutics, Graduate School of Pharmaceutical Sciences, Kyushu University, Fukuoka, Japan and [2]Department of Pharmaceutics, Teikyo University, Sagamiko, Sagamihara, Japan

Note: Supplementary data for this article are available at Cancer Research Online (http://cancerres.aacrjournals.org/).

F. Okazaki, N. Matsunaga, and S. Ohdo contributed equally to this work.

Corresponding Author: Shigehiro Ohdo, Department of Pharmaceutics, Graduate School of Pharmaceutical Sciences, Kyushu University, Fukuoka, 812-8582, Japan. Phone: 81-92-642-6610; Fax: 81-92-642-6614; E-mail: ohdo@phar.kyushu-u.ac.jp.

doi: 10.1158/0008-5472.CAN-10-0184

Published OnlineFirst July 14, 2010; DOI:10.1158/0008-5472.CAN-10-0184

In this study, we found that the circadian expression of *c-Myc*, which is controlled by the circadian clock, affects *TfR1* gene transcription in colon cancer cells. The levels of *TfR1* mRNA and protein exhibited a 24-hour oscillation in tumor cells implanted in mice. Thus, to evaluate the rhythmic function of TfR1 and the utility for TfR1-targeting cancer therapy, we investigated how the rhythmic variation in TfR1 production influenced the pharmacologic efficacy of TfR1-targeting liposomal DDS.

Materials and Methods

Animals and cells

Seven-week-old male BALB/c mice (Charles River Japan) were housed with lights on from 7:00 a.m. to 7:00 p.m. at a room temperature of 24 ± 1°C and a humidity of 60 ± 10% with food and water *ad libitum*. Colon 26 cells (Cell Resource Center for Biomedical Research, Tohoku University) were maintained in RPMI 1640 supplemented 10% fetal bovine serum (FBS) at 37°C in a humidified 5% CO_2 atmosphere. A 25-μL volume with 2×10^7 viable tumor cells was inoculated into the right hind footpad of each mouse. The tumor volume was estimated according to a formula that has been described previously (7). Tissue slices of the removed tumor masses were made, and the tumor tissue was confirmed histopathologically.

Experimental design

To assess the temporal expression profile of TfR1 in tumor cells, tumor masses were removed from individual tumor-bearing mice at six different time points (9:00 a.m., 1:00 p.m., 5:00 p.m., 9:00 p.m., 1:00 a.m., and 5:00 a.m.) 7 days after the implantation of tumor cells. The levels of *TfR1* protein and mRNA were measured by Western blotting analysis and quantitative reverse transcription-PCR (RT-PCR), respectively. To investigate how the rhythmic variation in *TfR1* expression occurs in tumor cells, the influence of CLOCK/BMAL1 and c-MYC on the transcriptional activity of the *TfR1* gene was assessed using luciferase reporter constructs containing wild-type E-box or mutated E-box of the mouse *TfR1* promoter, which was based on previous reports. To elucidate the role of c-MYC in the control of the rhythmic expression of *TfR1*, endogenous c-MYC in Colon 26 cells was downregulated by small interfering RNA (siRNA). The c-MYC–downregulated cells were treated with 50% FBS for 2 hours to synchronize their circadian clock, and the mRNA levels of *TfR1* were assessed at 44, 48, 52, 56, 60, 64, and 68 hours after 50% serum treatment. In the same manner as described above, the protein levels of c-MYC and CLOCK were assessed by Western blotting analysis. To explore the temporal binding of endogenous c-MYC and CLOCK to the E-box in the mouse *TfR1* gene, chromatin immunoprecipitation analysis was performed in individual tumor masses at 9:00 a.m. and 9:00 p.m. To investigate the function of the 24-hour oscillation of TfR1 expression, time-dependent changes in Pt internalization into tumor cells were assessed using Tf-coupled liposomes encapsulating oxaliplatin (Tf-NGPE L-OHP). The cultured Colon 26 cells were treated with 50% FBS as described above and then harvested for RNA extraction at 0, 6, 12, 18, and 24 hours after 50% FBS treatment. Nontreated Colon 26 cells harvested at the same time points were used as the control. At 6 or 18 hours after serum treatment, cells were exposed to Tf-NGPE L-OHP (L-OHP, 0.4 mg/mL) for 3 hours. The Pt content in the DNA was measured using an inductively coupled plasma mass spectrometer (ICP-MS). To explore the dosing time–dependent difference in the internalization of Pt into tumor cells *in vivo*, tumor-bearing mice were injected with a single dose of Tf-NGPE L-OHP at 9:00 a.m. or 9:00 p.m. Plasma and tumor DNA samples were collected only once from individual mice at 1, 3, and 6 hours after injection. The plasma concentration of Pt and its content in tumor DNA were measured as described above. Then, tumor volumes were measured throughout the duration of the experiment.

RT-PCR analysis

Total RNA was extracted using RNAiso (TaKaRa). The cDNAs of mouse *TfR1* (NM011638), *TfR2* (NM015799), *c-Myc* (NM010849), and β-*actin* (NM007393) were synthesized using PrimeScript Reverse Transcriptase (TaKaRa), and the synthesized cDNAs were amplified using GoTaq Green Master Mix (Promega). The PCR products were run on 2% agarose gels. After staining with ethidium bromide, the gel was photographed using Polaroid-type film. The density of each band was analyzed using NIH image software on a Macintosh computer. To evaluate the quantitative reliability of RT-PCR, kinetic analysis of the amplified products was performed to ensure that signals were derived only from the exponential phase of amplification, as previously described (7, 17). We evaluated the validity of our semiquantitative PCR methods using real-time PCR. cDNA was prepared by reverse transcription of total RNA. Real-time PCR analysis was performed on diluted cDNA samples with SYBR Premix Ex Taq Perfect Real-Time (TaKaRa) using a 7500 Real-time PCR system (Applied Biosystems). In addition, as confirmation of RNA extraction from each tumor cell sample, the expression level of *Vegf* mRNA was measured (Supplementary Data S1).

Western blotting analysis

Nuclear or cytoplasmic proteins in tumor masses were extracted using NE-PER Nuclear and Cytoplasmic Extraction Reagents (Pierce Biotechnology). The protein concentrations were determined using a BCA Protein Assay kit (Pierce Biotechnology). The lysate samples were separated on 6% or 10% SDS-polyacrylamide gels and transferred to polyvinylidene difluoride membranes. The membranes were reacted with antibodies against TfR1 (Zymed Laboratories), c-MYC, CLOCK, β-actin (Santa Cruz Biotechnology), or RNA pol II (Abcam). The immunocomplexes were further reacted with horseradish peroxidase–conjugated secondary antibodies and visualized using Super Signal Chemiluminescent Substrate (Pierce Biotechnology). The membranes were photographed using Polaroid-type film, and the density of each band was analyzed using NIH image software on a Macintosh computer.

Published OnlineFirst July 14, 2010; DOI:10.1158/0008-5472.CAN-10-0184

Construction of reporter and expression vectors

The 5′ flanking region of mouse *Tfr1* (from bp +16 to +436; +1 indicates the transcription start site) gene was amplified using Elongase Enzyme mix (Invitrogen) using DNA extracted from Colon 26 cells. PCR was performed using the forward primer 5′-AGTTGAGCTC(*Sac*I)GGCTTGGTGCAGCTCAGTTAGTAG-3′ and reverse primer 5′-ATGAGATATC(*Eco*RV)TAAATGTCCGTTGACACTAGTAACC-3′. The PCR products were purified and ligated into a pGL4 Basic vector (*Tfr1*-Luc). The sequence of the CACGTG E-box (bp +290 to +295) on *Tfr1*-Luc was mutated using a QuikChange site-directed mutagenesis kit (Stratagene). Expression vectors for mouse CLOCK, BMAL1, and c-Myc were constructed using cDNAs obtained from RT-PCR derived from mouse liver RNA. All coding regions were ligated into the pcDNA3.1 (+) vector (Invitrogen), as previously described (7). Protein expression levels from each expression vector in Colon 26 were assessed by Western blotting analysis (Supplementary Data S2).

Luciferase reporter assay

Colon 26 cells were seeded at 3×10^5 cells per well in six-well culture plates (BD Biosciences). After an 18-hour culture, the cells were transfected with 100 ng per well of reporter vector and 2 μg per well (total) of expression vector using Lipofectamine LTX reagent (Invitrogen). A 0.5-ng-per-well sample of phRL-TK vector (Promega) was also cotransfected as an internal control reporter. The total amount of DNA per well was adjusted by adding pcDNA3.1 vector (Invitrogen). At 24 hours posttransfection, cells were harvested and the cell lysate was analyzed using a dual-luciferase reporter assay system (Promega). The ratio of firefly luciferase activity to *Renilla* luciferase activity in each sample served as a measure of normalized luciferase activity.

Small interfering RNA

siRNA of the mouse *c-Myc* gene was designed using BLOCK-iT RNAi Designer (Invitrogen). The siRNA oligonucleotide sequences were as follows: siRNA control sense, 5′-UAGUGUGAGCACUGUGAUUCCUUGG-3′ and antisense 5′-CCAAGGAUCACAGUGCUCACACUA-3′; *c-Myc* siRNA sense 5′-UAGUCGAGGUC-AUAGUUCCUGUUGG-3′ and antisense 5′-CCAACAGGAACUAUGACCUCGACUA-3′. The oligonucleotides were transfected into Colon 26 cells at a final concentration of 20 nmol/L using Lipofectamine 2000 (Invitrogen).

Chromatin immunoprecipitation assays

Tumor masses were excised and treated with 1% formaldehyde for 5 minutes at room temperature to cross-link the chromatin, and the reaction was stopped by adding glycine to a final concentration of 0.125 mol/L. Each cross-linked sample was sonicated on ice and then incubated with antibodies against c-MYC, CLOCK, rabbit-IgG, or goat-IgG (Santa Cruz Biotechnology). Chromatin/antibody complexes were extracted using a protein G agarose kit (Roche). DNA was isolated using the Wizard SV Genomic DNA Purification System (Promega) and subjected to PCR using the following primers for the c-MYC binding site (E-box) of the *Tfr1* promoter region, forward 5′-GTGACTCCCTTGTCAG-3′ and reverse 5′-CCGTGACACTAGTAACC-3′. For PCR analysis, PCR products were amplified for 40 or 45 cycles. PCR products were run on an agarose (3%) gel, including 0.2 μg/mL ethidium bromide, and analyzed using the NIH image software.

Determination of L-OHP (Pt) concentration

Plasma samples were obtained by centrifugation at 3,000 rpm for 3 minutes and stored at −20°C until analysis. Tumor DNA was extracted using a Wizard Genomic DNA Purification kit (Promega). Measurements of the L-OHP (Pt) content in plasma and tumor DNA were made using ICP-MS at the Center of Advanced Instrumental Analysis, Kyushu University. ICP-MS is capable of detecting very small amounts of Pt. Plasma Pt concentration and its tumor DNA content were expressed as micrograms per milliliter and nanograms per nanogram of DNA, respectively.

Determination of the antitumor effect

Seven days after the inoculation of Colon 26 cells into mice, a single injection of Tf-NGPE L-OHP (L-OHP: 0, 7.5 mg/kg, i.v.) or vehicle (9% sucrose) was given to tumor-bearing mice at 9:00 a.m. or 9:00 p.m. This dosage of Tf-NGPE L-OHP was selected based on a preliminary study (Supplementary Data S3). In all mice, the tumor volumes were measured every 3 days throughout the duration of the experiment.

Statistical analysis

ANOVA was used for multiple comparisons, and Scheffe's test was used for comparison between two groups. A 5% level of probability was considered significant.

Results

Twenty-four-hour rhythm in the expression of TfR1 in Colon 26 tumor masses

Two subtypes of TfR have been identified: TfR1 and TfR2. In implanted Colon 26 cells, *Tfr1* but not *Tfr2* was detectable, although *Tfr2* was expressed in mouse liver (Supplementary Data S1B). The protein and mRNA levels of TfR1 in implanted Colon 26 cells showed a significant 24-hour rhythm, with higher levels during the early dark phase ($P < 0.05$; Fig. 1A and B). The increase and decrease in mRNA levels of *Tfr1* seemed to cause the rhythm of TfR1 protein in Colon 26 tumor masses.

Regulation of the 24-hour rhythm in the expression of *Tfr1* gene by c-MYC

Among these, c-MYC is a potent activator of *Tfr1* gene transcription in mice and humans, and the transactivation effect was elicited through binding to the CACGTG E-box located in the first intron region (18, 19). In addition, CLOCK/BMAL1 heterodimers also bind cooperatively to CACGTG E-box sequences and regulate the rhythmic expression of their target genes (2). Thus, to establish the relevance of the biological clock system on the expression of *Tfr1*, CLOCKΔ19 (CLOCK protein lacking transcriptional activity) was overexpressed in Colon 26 cells. Clock mutant mice have

Published OnlineFirst July 14, 2010; DOI:10.1158/0008-5472.CAN-10-0184

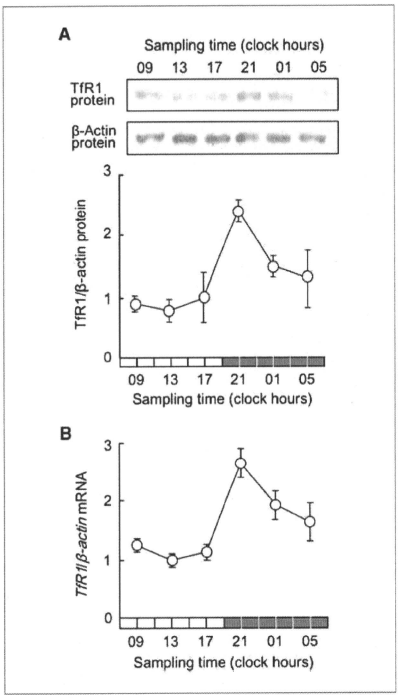

Figure 1. Twenty-four hour variation in the expression of TfR1 in Colon 26 tumor masses. A, temporal expression profile of TfR1 protein in tumor masses. The photographs show 24-h variation in TfR1 protein in implanted Colon 26 tumor cells. Cytoplasmic proteins were measured using each of the antibodies. Bottom, relative TfR1 protein levels. The data were normalized using β-actin as a control. Points, mean (n = 3, P < 0.01, ANOVA); bars, SEM. B, temporal expression profile of *TfR1* mRNA in tumor masses. The data are normalized using β-*actin* as a control. Points, mean (n = 6, P < 0.01, ANOVA); bars, SEM.

a point mutation in exon 19 of the *Clock* gene and exhibit low-amplitude rhythms in the expression of various genes (20). *TfR1* and *c-Myc* expression levels were low in CLOCKΔ19 overexpressing Colon 26 cells (Supplementary Data S4). Next, we tested whether these transcription factors participate in regulation of the rhythmic expression of *TfR1* gene in Colon 26 cells. Cotransfection of *TfR1*-Luc with c-MYC expression constructs resulted in an 8.1-fold increase in promoter activity, whereas CLOCK/BMAL1 had little effect on the transcriptional activity of the *TfR1* gene (Fig. 2B). The transactivation effect of c-MYC on *TfR1* reporters was dependent on the E-box element located from bp +290 to +295 because mutation of the CACGTG sequence to AAGCTT reduced transcriptional activation by c-MYC from 8.1- to 1.5-fold.

Several compounds and high concentration serum have been shown to induce and/or synchronize circadian gene expression in cultured cells (21). Thus, to elucidate the role of c-MYC in the circadian regulation of *TfR1* expression, the temporal expression profiles of *TfR1* mRNA in c-MYC–downregulated Colon 26 cells were investigated after 50% FBS treatment. Brief exposure of control scrambled siRNA-transfected cells to 50% FBS resulted in the oscillation of *TfR1* mRNA levels with a period length of ~24 hours (Fig. 3A). On the other hand, the protein levels of c-MYC were decreased and the mRNA levels of *TfR1* failed to show a significant 24-hour oscillation after the treatment of *c-Myc* siRNA–transfected cells with 50% FBS (Fig. 3B and C). These results suggested that c-MYC is required for generating the time-dependent variation in *TfR1* mRNA expression.

The transcription of *c-Myc* is regulated by components of the circadian clock, and its mRNA levels in mouse liver and bones have been shown to exhibit a significant 24-hour oscillation (22). The protein levels of c-MYC in Colon 26 cells implanted in mice also showed obvious 24-hour oscillations with higher levels around the early dark phase and lower levels during the early light phase, whereas there was no obvious 24-hour variation in the protein levels of CLOCK in the tumor

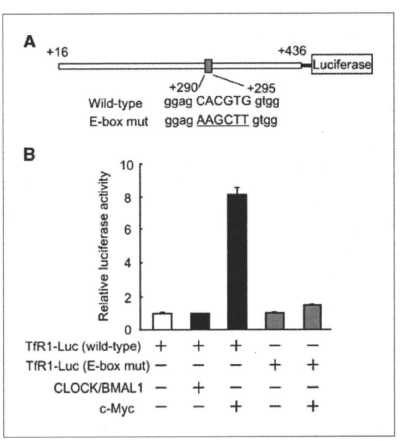

Figure 2. Influence of CLOCK/BMAL1 and c-MYC on transcription of the mouse *TfR1* gene. A, schematic representation of the mouse *TfR1* promoter. The numbers on both sites, the distance (bp) from the transcription start site (+1) included in the luciferase reporter construction. The numbers of nucleotide residues below the box, the positions of the E-box. The underlined nucleotide residues, the mutated sequence of the E-box. B, wild-type or E-box–mutated *TfR1* gene reporter plasmids (*TfR1*-Luc) were cotransfected with expression constructs encoding CLOCK/BMAL1 or c-MYC. Columns, mean (n = 3); bars, SEM.

Published OnlineFirst July 14, 2010; DOI:10.1158/0008-5472.CAN-10-0184

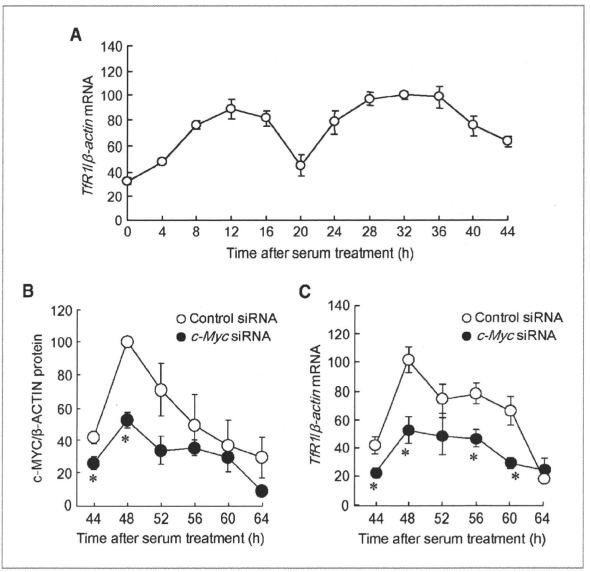

Figure 3. Influence of the downregulation of c-MYC on the rhythmic expression of *TfR1* mRNA in Colon 26 cells. A, temporal accumulation of *TfR1* mRNA in Colon 26 cells after 50% serum shock. The data are normalized using β-*actin* as a control. Points, mean ($n = 3$, $P < 0.01$, ANOVA); bars, SEM. Data are plotted relative to the 0-h value after 50% serum shock. B, temporal accumulation of c-MYC protein in control cells or c-Myc knockdown cells after 50% serum shock. Colon 26 cells were transfected with scrambled siRNA (control siRNA) or specific siRNA for c-Myc (c-Myc siRNA). Crude cell extracts were measured by Western blotting analysis. The data were normalized using β-actin as a control. Points, mean ($n = 3$, control cells; $P < 0.01$, ANOVA); bars, SEM. *; $P < 0.05$, when compared with the value for the control siRNA group at the corresponding times. C, temporal accumulation of *TfR1* mRNA in control cells or *c-Myc* knockdown cells. The mRNA levels of *TfR1* were determined at the indicated time points after serum treatment. Points, mean ($n = 3$, control cells; $P < 0.01$, ANOVA); bars, SEM. *, $P < 0.05$, when compared with the value for the control siRNA group at the corresponding times.

cells (Fig. 4A). The results of chromatin immunoprecipitation analysis revealed that endogenous c-MYC in Colon 26 cells bound to the E-box element in the intron region of *TfR1* gene (Fig. 4B). Of particular note, the binding amounts of c-MYC increasedat the time of day corresponding to the peak of *TfR1* mRNA expression (see Fig. 1B), suggesting that the time-dependent binding of c-MYC to the E-box in *TfR1* gene underlies its rhythmic expression. In addition, the mRNA levels of a prototypical c-MYC–regulated gene, telomerase reverse transcriptase (23), in Colon 26 cells implanted in mice also showed time-dependent variation (Supplementary Data S5).

Relationship between the rhythmic expression of TfR1 and time dependency of Pt incorporation into tumor DNA

Tf-NGPE L-OHP is a transferrin-conjugated liposome encapsulating L-OHP, a diaminocyclohexane Pt antitumor agent, which forms adducts with DNA. Tf-NGPE L-OHP binds to TfR, which is expressed on the plasma membrane and can internalize Pt into the cell.[3] Thus, to explore the function of internalization into the cell through transferrin in the rhythmic expression of TfR1, we investigated the temporal profile of *TfR1* gene expression and incorporation of Pt into tumor DNA in synchronized and desynchronized Colon 26 cells. A brief exposure of cultured Colon 26 cells to 50% FBS medium for 2 hours induced an oscillation in the expression of *TfR1* mRNA (Fig. 5A). The mRNA levels of *TfR1* peaked at 18 hours after treatment of the cells with 50% FBS. The oscillation of *TfR1* mRNA levels was also found on day 3 after serum treatment (see Fig. 3). The amount of Pt incorporated into the DNA of serum-shocked cells after treatment with Tf-NGPE L-OHP increased significantly at the time point corresponding to the peak in the level of TfR1 protein ($P < 0.05$; Fig. 5B). In contrast, in nontreated cells, neither the mRNA and protein levels of TfR1 nor Pt incorporation showed significant time-dependent variations (Fig. 5A and B), suggesting that the oscillation in the

[3] Our unpublished data.

Published OnlineFirst July 14, 2010; DOI:10.1158/0008-5472.CAN-10-0184

expression of TfR1 underlies the time-dependent change in Pt incorporation into tumor DNA.

Influence of dosing time on the ability of Tf-NGPE L-OHP to inhibit tumor growth

The plasma Pt concentration decreased gradually after a single injection of 7.5 mg/kg Tf-NGPE L-OHP (i.v.) at both dosing times, but the Pt concentration in plasma at 3 hours after Tf-NGPE L-OHP injection was significantly higher in mice injected with the drug at 9:00 a.m. than at 9:00 p.m. (Fig. 6A, left). On the other hand, Pt incorporation into DNA in tumor cells at 3 and 6 hours after Tf-NGPE L-OHP injection was significantly higher in mice injected with the drug at 9:00 p.m. than at 9:00 a.m. (Fig. 6A, right). We also attempted to determine the Pt contents in tumor DNA at over 6 hours after Tf-NGPE L-OHP injection, but accurate assessment was difficult, probably due to L-OHP–induced apoptotic or necrotic tumor cell death.

A significant antitumor effect of Tf-NGPE L-OHP was observed when tumor-bearing mice were injected i.v. with a single dose of 7.5 mg/kg L-OHP (Supplementary Data S3). Thus, the dosage was set at 7.5 mg/kg to investigate whether the antitumor effect of Tf-NGPE L-OHP was altered depending on its dosing time. The growth of tumor cells was significantly suppressed by the administration of Tf-NGPE L-OHP (7.5 mg/kg, i.v.). The antitumor effects were more potent in mice injected with the drug at 9:00 p.m. than in those that received it at 9:00 a.m. (Fig. 6B). Fifteen days after injection of the drug, the tumor volume in mice injected with Tf-NGPE L-OHP at 9:00 p.m. was significantly smaller than that in mice injected at 9:00 a.m. ($P < 0.05$).

Discussion

TfR1 is a key cell surface molecule that regulates the uptake of iron-bound transferrin (8). It has been shown that correlation exists between the number of surface TfR1 and the rate of cell proliferation. TfR1 expression is higher in tumor cells than in normal cells. Thus, intracellular targeting using iron-saturated Tf as a ligand for TfR-mediated endocytosis has attracted attention. In this study, the protein abundance of TfR1 on Colon 26 tumor cells implanted in mice showed a clear 24-hour oscillation. The rhythmic phase of TfR1 protein

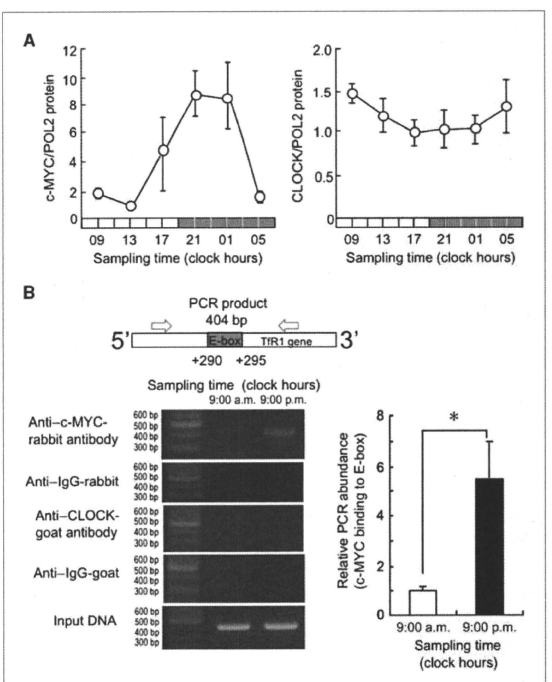

Figure 4. Time-dependent changes in the binding of endogenous c-MYC to the E-box element in the *TfR1* gene. A, temporal expression profiles of protein levels of c-MYC and CLOCK in implanted Colon 26 tumor masses. POL2 protein was used as an internal control whose expression was constant throughout the day. The data are normalized using POL2 as a control ($P < 0.01$, ANOVA). CLOCK protein did not show an obvious variation. Points, mean ($n = 3$); bars, SEM. B, left, temporal profiles of the binding of endogenous c-MYC to the *TfR1* gene in Colon 26 cells implanted in mice. Right, the quantification of temporal changes in the binding of c-MYC to the *TfR1* gene in Colon 26 cells implanted in mice. The mean value of each assay at 9:00 a.m. was set at 1. Columns, mean ($n = 3$); bars, SEM. *; $P < 0.05$ for the comparison between the two groups.

Published OnlineFirst July 14, 2010; DOI:10.1158/0008-5472.CAN-10-0184

paralleled that of its mRNA levels. However, the mechanisms of transcriptional rhythm of TfR1 were unclear.

The molecular circadian clock operates at a cellular level and coordinates a wide variety of physiologic processes (24). CLOCK/BMAL1 heterodimers activate the transcription of *Per, Cry*, and *Dec* genes through CACGTG E-box enhancer elements (8). The results of luciferase reporter assays and chromatin immunoprecipitation experiments revealed that the CACGTG E-box located in the first intron of the mouse *TfR1* gene was unable to respond to CLOCK/BMAL1 heterodimers. In contrast, as reported previously (19), c-MYC could bind to the E-box of the mouse *TfR1* gene and activate its transcription. The amount of endogenous c-MYC protein binding to the mouse *TfR1* gene E-box fluctuated in a time-dependent manner. The binding of c-MYC to the E-box increased at the time corresponding to the peak of *TfR1* mRNA expression, suggesting that c-MYC acts as a regulator of circadian expression of the *TfR1* gene in Colon 26 tumor cells. This hypothesis was also supported by the present findings that the amplitude of the *TfR1* mRNA rhythm in serum-shocked Colon 26 cells was decreased by the down-regulation of c-MYC. On the other hand, CLOCK protein did not bind to the *TfR1* gene E-box. This may account for the unresponsiveness of the *TfR1* gene to CLOCK/BMAL1 heterodimers. The sequence surrounding the E-box and its location had a marked influence on the transcriptional activity of CLOCK/BMAL1 (6). In fact, a CT-rich *cis*-acting element of the mouse vasopressin gene confers robust CLOCK/BMAL1 responsiveness on an adjacent E-box (25). The absence of such a CT-rich *cis*-acting element around the E-box may result in the inability of CLOCK/BMAL1 to transactivate the mouse *TfR1* gene.

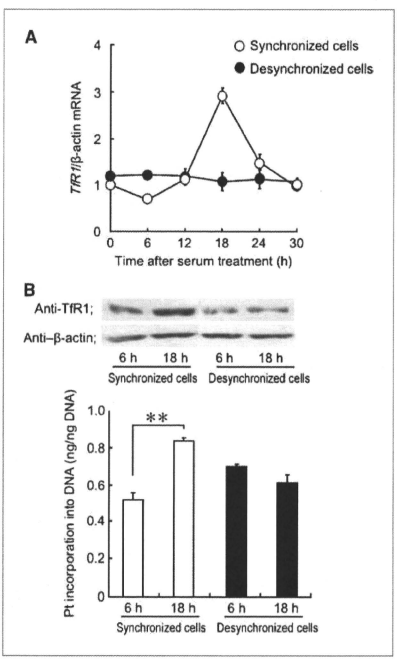

Figure 5. Influence of rhythmic changes in the expression of TfR1 on intratumoral delivery of L-OHP by Tf-NGPE liposomes. A, the temporal expression profile of *TfR1* mRNA in synchronized (○) or unsynchronized (●) Colon 26 cells. Cultured Colon 26 cells were synchronized by exposure to 50% FBS for 2 h. Points, mean ($n = 3$, synchronized cells; $P < 0.05$, ANOVA); bars, SEM. B, the photographs show temporal expression of TfR1 protein in synchronized or unsynchronized Colon 26 cells. Bottom, that temporal profile of Pt incorporation into DNA in synchronized or unsynchronized Colon 26 cells. Cells were exposed to Tf-NGPE L-OHP (L-OHP: 0.4 mg/mL) for 3 h at 6 or 18 h after the serum treatment, and then the amounts of Pt incorporated into tumor DNA were measured. Columns, mean ($n = 3$); bars, SEM. *, $P < 0.05$ for the comparison between the two time points.

Because the rhythmic phase of c-MYC protein abundance in Colon 26 cells correlated with the time dependency of its binding to the *TfR1* gene E-box, the oscillation in c-MYC protein levels may cause the 24-hour rhythm in the expression of downstream genes by rhythmic binding to their DNA response elements. In fact, *mTERT* mRNA in implanted Colon 26 tumor also showed time-dependent variation. In addition, *c-Myc* is regulated by clock genes, as indicated by previous results (26). *TfR1* and *c-Myc* expression levels were low in CLOCKΔ19-overexpressing Colon 26 cells. Although the E-box of the *TfR1* gene did not respond to CLOCK/BMAL1, the molecular components of the circadian clock may indirectly regulate the expression of the *TfR1* gene in Colon 26 cells.

It was reported previously that L-OHP could accumulate in tumor masses following delivery using Tf-PEG liposomes (16). TfR-targeting liposomes also bind to TfR on tumor cell surfaces and are internalized into the cells by receptor-mediated endocytosis. In this study, to evaluate the function of the 24-hour oscillation in TfR1, Tf-NGPE liposomes were used as a targeting carrier for intratumoral delivery of L-OHP. This TfR-targeting liposomal DDS exhibited similar pharmacokinetic properties to Tf-PEG liposomes, and i.v. administration of L-OHP encapsulated within Tf-NGPE liposomes lead to the accumulation of a high concentration of L-OHP in tumors as much as Tf-PEG liposomes.[4] The amount of Pt in tumor DNA after Tf-NGPE L-OHP injection increased at the times of day when TfR1 was abundant on the tumor surface in this study. This notion was also supported by *in vitro* findings that the time dependency of Tf-NGPE liposome–delivered L-OHP into tumor cells disappeared in the absence of the oscillation in TfR1 expression. These findings suggest that the oscillation in the expression of TfR1 underlies the dosing time–dependent changes in the internalization into

[4] Our unpublished data.